Journal of Nuclear Materials 484 (2017) 307–323

Contents lists available at ScienceDirect

Journal of Nuclear Materials

journal homepage: www.elsevier.com/locate/jnucmat

Instant release of fission products in leaching experiments with high burn-up nuclear fuels in the framework of the Euratom project FIRST- Nuclides

K. Lemmens [a, *], E. González-Robles [b], B. Kienzler [b], E. Curti [c], D. Serrano-Purroy [d], R. Sureda [e], A. Martínez-Torrents [e], O. Roth [f], E. Slonszki [g], T. Mennecart [a], I. Günther-Leopold [c], Z. Hózer [g]

[a] Waste and Disposal Expert Group, Belgian Nuclear Research Centre (SCK•CEN), Boeretang 200, 2400 Mol, Belgium
[b] Karlsruhe Institute of Technology Institute for Nuclear Waste Disposal (KIT-INE), PO Box 3640, D-76021 Karlsruhe, Germany
[c] Laboratory for Waste Management, Nuclear Energy and Safety Dept., Paul Scherrer Institute, 5232 Villigen PSI, Switzerland
[d] European Commission, DG Joint Research Centre - JRC, Directorate G - Nuclear Safety & Security, Department G.III, PO Box 2340, D-76125 Karlsruhe, Germany
[e] CTM Centre Tecnològic, Plaça de la Ciència 2, 08243 Manresa, Spain
[f] Studsvik, Nuclear AB, 611 82 Nyköping, Sweden
[g] Magyar Tudományos Akadémia Energiatudományi Kutatóközpont (MTA EK), PO Box 49, H-1525 Budapest, Hungary

HIGHLIGHTS

- Leach tests were performed to study the instant release of fission products from high burn-up UO_2 fuels and one MOX fuel.
- In these tests, the fission gas release given by the operator was a pessimistic estimator of the iodine and cesium release.
- Iodine and cesium release is proportional to linear power rating beyond 200 W cm^{-1}.
- Closure of the fuel-cladding gap at high burn-up slows down the release.
- The release rate decreases following an exponential equation.

GRAPHICAL ABSTRACT

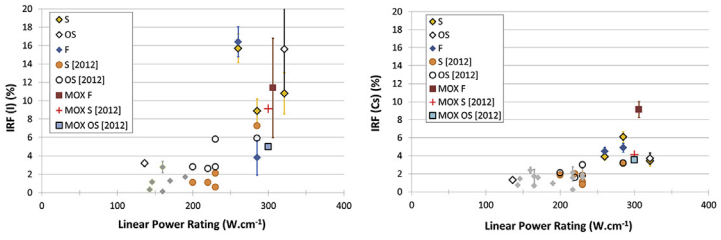

ARTICLE INFO

Article history:
Received 28 June 2016
Received in revised form
25 October 2016
Accepted 27 October 2016
Available online 1 November 2016

Keywords:
Spent nuclear fuel
Static leaching
Instant release fraction
FIRST-Nuclides

ABSTRACT

The instant release of fission products from high burn-up UO_2 fuels and one MOX fuel was investigated by means of leach tests. The samples covered PWR and BWR fuels at average rod burn-up in the range of 45 −63 GWd/t_{HM} and included clad fuel segments, fuel segments with opened cladding, fuel fragments and fuel powder. The tests were performed with sodium chloride − bicarbonate solutions under oxidizing conditions and, for one test, in reducing Ar/H_2 atmosphere. The iodine and cesium release could be partially explained by the differences in sample preparation, leading to different sizes and properties of the exposed surface areas. Iodine and cesium releases tend to correlate with FGR and linear power rating, but the scatter of the data is significant. Although the gap between the fuel and the cladding was closed in some high burn-up samples, fissures still provide possible preferential transport pathways.

Acronyms: FGR, Fission gas release; IRF, Instant release fraction; LPR, Linear power rating; SNF, Spent nuclear fuel.

* Corresponding author.
E-mail address: klemmens@sckcen.be (K. Lemmens).

http://dx.doi.org/10.1016/j.jnucmat.2016.10.048

1. Introduction

The Spent Nuclear Fuel (SNF) generated by thermal neutron irradiation of UO_2 or Mixed UO_2-PuO_2 oxide (MOX) fuels in nuclear power plants is a heterogeneous material, of which the structure, chemical composition and properties depend on the burn-up and in-pile irradiation history. The properties of irradiated fuels have been investigated since several decades, and comprehensive standard literature is available [1–3]. In an irradiated UO_2 fuel rod from Light Water Reactors (LWR), one can distinguish several structural-compositional elements: the zircaloy cladding, the gap between the cladding and the fuel (some tens of micrometers in thickness), and the fuel pellet itself, which is characterized by radial cracks formed as a result of the steep radial temperature gradient [4]. On a microscopic scale, the fuel consists of porous micro sized UO_2 grains containing sparse metal particles (known as "epsilon" particles). For the evaluation of leach experiments, structures representing potential pathways accessible to aqueous solutions are important. These include the fuel-cladding gap, the radial and longitudinal cracks, open pores in the matrix and fuel grain boundaries. In the case of SNF with an average burn-up higher than 40 GWd/t_{HM}, the formation of a rim structure [5–7] is observed, showing a distinctly smaller average grain size and increased porosity in comparison to the inner parts of the fuel. Chemically, the fission products in the SNF can be classified into four main groups [8]: (1) fission gases (mainly Kr, Xe); (2) fission products forming metallic particles (e.g. Tc, Ru, Pd); (3) fission products forming discrete oxides (e.g. Ba, Zr); (4) fission products dissolved as solid solution in the UO_2 matrix (e.g. REE, Sr). Some elements may partition in different phases, e.g. molybdenum plays a role in buffering the oxygen potential of the fuel and can coexist in metallic and oxide phases. The behavior of iodine and cesium, which are major contributors of fast release in leach tests, cannot be entirely rationalized in terms of the above scheme. During reactor operation, these elements may behave like fission gases due to their low boiling points, but they may also form a soluble phase (CsI), which is rapidly dissolved upon contact with water. Because the cesium concentration (in mole) surmounts the iodine concentration, cesium may also be associated to UO_2 and iodine may partition significantly in the fission gas phase.

When the SNF is disposed of in an underground repository, the radionuclides may gradually be released after failure of the canister and subsequent water ingress. The release rate of radionuclides differs depending on their chemical properties, their chemical speciation in the fuel, as well as the location where they are segregated within the SNF. Elements such as cesium and iodine are mainly volatile during irradiation of the fuel and undergo diffusion processes in the thermal gradient of the fuel rods. For fuel operated in high-power conditions (typically above 1100–1200 °C) these elements tend to segregate in the cooler regions at the pellet periphery and in the fuel/cladding gap. Typically, an operational distinction is made between the release from the fuel grains, from the grain boundaries and from the gap and cracks [9]. The release of fission products incorporated in the UO_2 grains (matrix dissolution) is very slow, especially under reducing conditions, as radiolytic fuel oxidation is suppressed [10,11]. The release of soluble segregated elements from the accessible gap, cracks and grain boundaries is fast. Most of their inventory is released within a few months or even days. The quantity of these rapidly released inventories normalized to the total nuclide inventories is commonly called the Instant Release Fraction (IRF) in safety assessment studies. Because some of the involved radionuclides are long-lived, and geochemically mobile (especially ^{129}I, ^{135}Cs, ^{36}Cl), they can significantly contribute to or even dominate the calculated dose exposure [12,13]. First measurements of the fast release were performed on low burn-up CANada Deuterium Uranium (CANDU) fuel [9,14,15]. Later, several European projects investigated the fast release mainly from Pressurized Water Reactor (PWR) UO_2 fuel [16–20].

Recently, experimentally determined fast release results were correlated with Fission Gas Release (FGR) [21]. The FGR can be measured directly by different methods [22,23] or calculated with relatively good precision [24,25]. It depends strongly on the operating conditions, especially on the burn-up, ramping and power rating. However, the correlation between burn-up, fast release and FGR proved to be weak due to the considerable scatter of the data and has therefore a low predicting power. Johnson et al. [21] suggested that linear power rating could be a more appropriate parameter to predict fast release. Up to date, the experimental database supporting this suggestion was small, partly due to the limited knowledge of power rating values for the investigated samples. Moreover, because the utilities tend nowadays to increase the burn-up in order to optimize energy production, it is particularly important to extend the experimental IRF database to such high burn-up fuels and to test correlations with well-known reactor operational parameters.

For this purpose, a common experimental program was set up by a group of laboratories, in the framework of the FP7 Collaborative Project FIRST-Nuclides (Fast/Instant Release of Safety Relevant Radionuclides from Spent Nuclear Fuel, 2012–2014), carried out during the 7th European Union's Research and Innovation funding program (FP7) [26]. The experimental investigations included the gas release, rim and grain boundary diffusion processes, and leach tests, for quantification of the fast release of activation and fission products into the aqueous phase, with – to the extent possible – determination of their chemical speciation. The leach tests were performed with well characterized spent nuclear fuel samples by Karlsruhe Institute of Technology (KIT) Germany, Joint Research Centre – Directorate G (by the formerly called Institute for Transuranium Elements (ITU)), Paul Scherrer Institut (PSI) Switzerland, Studiecentrum voor Kernenergie - Centre d'Étude de l'énergie Nucléaire (SCK•CEN) Belgium, Fundació Centre Tecnològic de Manresa (CTM) Spain, and Studsvik Nuclear AB (STUDSVIK) Sweden. The leach tests were performed with fuels from pressurized water reactors or Boiling Water Reactors (BWR) with average rod burn-ups ranging from 42 to 63 GWd/t_{HM}. The leach tests were complemented by analysis of release rates of relevant radioisotopes from damaged and leaking VVER (Vodo-Vodyanoi Energetichesky Reaktor) fuel elements during their storage in a water pool. These fuels had been previously irradiated in a Hungarian pressurized water reactor. This paper summarizes the results of the leach experiments and attempts to establish correlations to improve the IRF estimations for high burn-up UO_2 fuel.

2. Experimental

Leaching tests were done with samples from various UO_2 fuels and one type of MOX fuel, irradiated either in PWR's or BWR's. The main characteristics of the investigated SNF samples are shown in Tables 1 and 2. In these tables, the average rod burn-up is listed as reported by the utilities, based on core physics calculations and the plant thermal output ('rod ave-cal' in Tables 1 and 2). The local burn-up of the tested sample can be different, and is given when this information is available ('loc' in Tables 1 and 2). The local burn-up values are either calculated by core physics calculations ('loc-cal' in Tables 1 and 2), measured by gamma scanning ('loc-gam' in Tables 1 and 2), or by dissolution of the sample and radiochemical analysis ('loc-diss' in Table 1). The linear power rating (LPR) distinguishes the rod average LPR ('rod ave' in Tables 1 and 2),

referring to the entire rod over all burning cycles, the rod maximum LPR ('rod max' in Tables 1 and 2), referring to the maximum LPR reached by the entire rod over all burning cycles, and similar values for the local LPR, referring to the sample position. The 'loc-ave' LPR in Tables 1 and 2 thus refers to the local average over all burning cycles, and the 'loc-max' LPR refers to the local maximum LPR reached during the burning cycles.

The fuel samples for the leach tests were prepared as follows: (1) fuel segments with their cladding were cut from the fuel rods; these tests with clad fuel segments will be indicated as 'Segment' (S), (2) the cladding of segments was opened and separated from the fuel fragments but leached together with them; these tests with declad fuel segments are indicated as 'Open Segment' (OS), (3) mm-size fuel fragments were separated and leached without cladding, indicated as 'Fragments' (F), (4) fuel powder with average sizes varying from approximately 10 to 90 μm was leached without cladding, indicated as 'Powder' (P); tests were done separately with powder from the outer zone (P_{Out}), enriched in high burn-up structure, and from the core zone of the pellet (P_{Core}). The definitions used here may be different in other studies. For example, Ekeroth et al. [27] used the term 'Fragments' for what is called here 'Open Segment'. An overview of the samples that were tested for each fuel type is given in the last column of Tables 1 and 2.

Figs. 1–5 show pictures of the various types of samples.

The fuel segments with cladding were cut in three different ways: (1) 20–24 mm long segments containing one intact and two half pellets, from mid-pellet to mid-pellet (SCK•CEN, PSI, Studsvik), (2) 10 mm long segments containing one intact pellet, cut at the pellet-pellet interface (KIT), (3) short in-pellet segments with a length of 2.5–2.8 mm (CTM and ITU).

The specific surface area of the samples was very diverging, but in many cases not well known. For powders, the specific surface area was much larger than for fuel segments. It was estimated between 2×10^2 and 5×10^2 $cm^2\ g^{-1}$ for the BWR42 and BWR54 powders, and - based on the geometry - between 2 and 4 $cm^2\ g^{-1}$ for the short segments (S), assuming that the lateral surface was not exposed because of the closed gap. For the long segments, assuming that the lateral surface is also exposed, the specific surface area should be larger. These estimations, however, neglect the unknown contribution of open fissures to the total surface area exposed to solution. For the fuel fragments (F) and opened segments (OS), the specific surface area must lie between the high value for the powders and the low value for the clad pellets, but a more accurate estimation cannot be given.

The prepared fuel samples were immersed in a leachant, consisting of 19 mM NaCl and 1 mM $NaHCO_3$. Studsvik used a slightly different composition (10 mM NaCl and 2 mM $NaHCO_3$). The leaching apparatus of PSI and SCK•CEN was identical, consisting of 150 ml glass columns filled with the fuel sample and the leachant. A complete solution renewal was foreseen only for the first samplings (twice at SCK•CEN, once at PSI). Afterwards, small samples were taken at regular time intervals. KIT followed a similar sampling strategy, with one complete renewal of the solution after the first sampling, in an autoclave with 220 ml volume, allowing also gas sampling. In the leaching set-up of CTM, ITU and Studsvik, the solution was completely replaced for each sampling. All tests were performed in oxidizing (aerobic) conditions, except for the tests at KIT (fuel SBS1108), which were performed under Ar/H_2 atmosphere with a H_2 partial pressure of 3.2 bar and a total pressure of 40 bar.

Test durations of up to 1 year were planned. The leachates were analyzed for a number of radionuclides, depending on the techniques available in the participating laboratories. All laboratories provided measurements for cesium and most of them also for iodine. Several laboratories measured additional elements/radioisotopes, such as ^{14}C, Se, Sr, Tc, Pd, Sn, Mo, and Rb. Solid state analyses were carried out at Studsvik, where the Se distribution in a UO_2 pellet was measured by laser ablation [28] and at PSI, where micro-XRF and micro-XANES analyses were carried out to determine the primary distribution and oxidation state of Se in selected non-leached SNF samples [29,30]. More precise descriptions of the experimental procedures adopted for the leaching experiments and results obtained for radioisotopes other than Cs and I are given in specific papers provided by each institution: ITU [31], CTM [32], KIT [33–35] PSI [29,30,36], Studsvik [37,38] and SCK•CEN [39]. Another partner of FIRST-Nuclides (Magyar Tudományos Akadémia Energiatudományi Kutatóközpont (MTA EK) Hungary) has collected and interpreted the isotopic release data from damaged and leaking VVER fuel rods [40]. A benchmark of the analytical methods used by the different laboratories was not foreseen within the FIRST-Nuclides project.

3. Results and comparison with previous experiments

3.1. Definition of IRF

The experiments provide an important dataset of new SNF leaching data, especially for I and Cs. These data are expressed as Fraction of Inventory in the Aqueous Phase (FIAP), which indicates

Table 1
Characteristics of the PWR fuels used in the leach tests of FIRST-Nuclides. Both the average rod burn-up ('rod ave') and the local burn-up at the sample position ('loc') are given (when available). The burn-up data were either calculated ('rod ave-cal' or 'loc-cal'), or determined by gamma scanning ('loc-gam'), or by dissolution and radiochemical analyses ('loc-diss'). The linear power rating (LPR) distinguishes the average rod LPR over all burning cycles ('rod ave'), the rod maximum LPR ('rod max'), the local average over all burning cycles ('loc-ave'), and the local maximum LPR reached during the burning cycles ('loc-max'). The last column shows the type of samples that was tested (S = clad fuel segment, OS = opened fuel segment, F = fuel fragments). The fuels are listed following increasing Fission Gas Release (FGR).

Institution	Enrichment (% ^{235}U)	Rod type and reactor	Identification	Burn-up ($GWd.t_{HM}^{-1}$)	LPR ($W.cm^{-1}$)	FGR (%)	Sample type
Studsvik	2.8	Standard+ 8% Gd (Vandellòs)	VG81	54.4 (rod ave-cal) 55.7 (loc-gam)	136 (rod ave)	2.2 ± 0.07	OS
KIT	3.8	Test NIKUSI production[c] (KKG)	SBS1108	50.4 (rod ave-cal)	260 (rod ave) 340 (rod max)	8.34 ± 0.91	S, F
PSI	4.3	Test (KKG)	KKG-UO_2	56.6 (rod ave-cal) 65.1 (loc-gam)	285 (rod ave)	13.2 ± 0.5	S, F
SCK·CEN	4.3	Standard (Tihange 1)	D05	50.5 (rod ave-cal) 54.6 (loc-diss) 54.3 (loc-cal)	321 (loc-ave)[b] 400 (loc-max)	14.1 ± 0.9	S, OS
PSI	5.5% Pu_{fiss}[a]	Test (KKG)	KKG-MOX	63 (rod ave-cal) 72.5 (loc-gam)	306 (rod ave) 430 (rod max)	26.7 ± 0.6	F

[a] MOX fuel.
[b] 350–400 W/cm (1st cycle), 250–300 W/cm (2nd cycle).
[c] This fuel has as a smaller grain size than standard UO_2 fuel [56].

Table 2
Characteristics of the BWR fuels used in the leach tests of FIRST-Nuclides. Both the average rod burn-up ('rod ave') and the local burn-up at the sample position ('loc') are given (when available). The burn-up data were either calculated ('rod ave-cal'), or determined by gamma scanning ('rod ave-gam' or 'loc-gam'). The linear power rating (LPR) distinguishes the average rod LPR over all burning cycles ('rod ave'), the rod maximum LPR ('rod max'), the local average over all burning cycles ('loc-ave'), and the local maximum LPR reached during the burning cycles ('loc-max'). The last column shows the type of samples that was tested (S = clad fuel segment, OS = opened fuel segment, F = fuel fragments, P = fuel powder from the core and from the outer zone of the pellet). The fuels are listed following increasing Fission Gas Release (FGR).

Institution	Enrichment (% ^{235}U)	Rod type and reactor	Identification	Burn-up ($GWd.t_{HM}^{-1}$)	LPR ($W.cm^{-1}$)	FGR (%)	Sample type
Studsvik	4.1	Standard Cr_2O_3/Al_2O_3 doped UO_2 (Oskarshamn 3)	C1	59.1 (rod ave-cal) 56 (rod ave-gam) 61.1 (loc-gam)	190 (rod ave)	1.4 ± 0.03	OS
Studsvik	4.25	Standard (Olkiluoto)	D07	50.2 (rod ave-cal) 59.3 (loc-gam)	143 (rod ave) 145 (loc-ave)	1.6 ± 0.05	S
PSI	3.9	test (KKL)	KKL-UO_2	57.5 (rod ave-cal) 60.4 (loc-gam)	160 (rod ave) 270 (rod max)	2.26± 0.1	S, F
JRC-ITU	3.7	Standard (n.a.)[a]	BWR42	42 (rod ave-cal) 45 (loc-gam)	217 (rod ave) 293 (rod max)	2.3± 0.2	S, P
Studsvik	3.5	Standard (Oskarshamn 3)	5A2	57.1 (rod ave-cal) 60.5 (loc-gam)	170 (rod ave)	2.4 ± 0.03	OS
Studsvik	4.25	Standard (Olkiluoto)	L04	54.8 (rod ave-cal) 53.4 (rod ave-gam) 65.7 (loc-gam)	146 (rod ave) 162 (loc-ave)	3.1 ± 0.03	S
CTM	4.2	Standard (n.a.)[a]	BWR54	54 (rod ave-cal) 58 (loc-gam)	165 (loc-ave) 275 (loc-max)	3.9± 0.4	S, P

[a] Information about reactor not available.

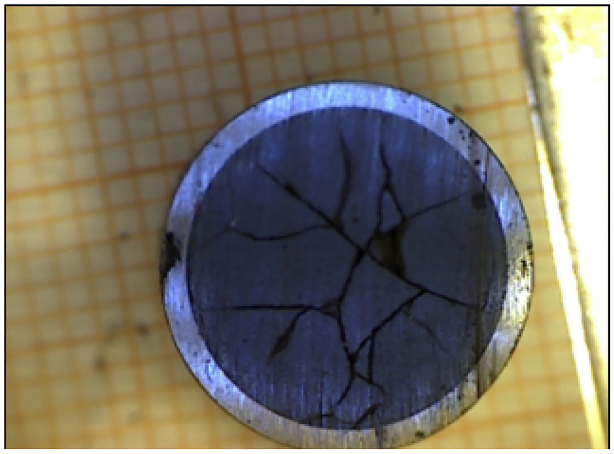

Fig. 1. Clad fuel segment (fuel SBS1108).

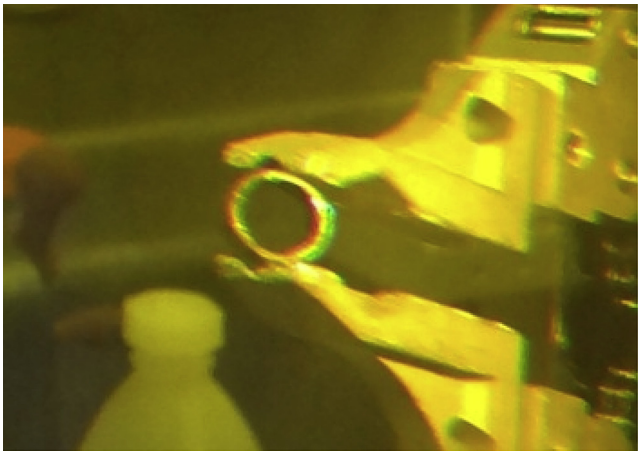

Fig. 3. Transversally opened fuel segment after pushing out the fuel (fuel D05). The emptied cladding is leached together with the fuel fragments.

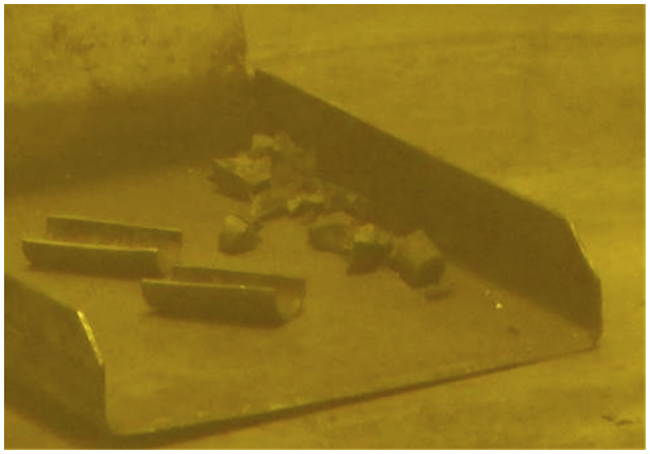

Fig. 2. Longitudinally opened fuel segment (fuel KKL-UO_2).

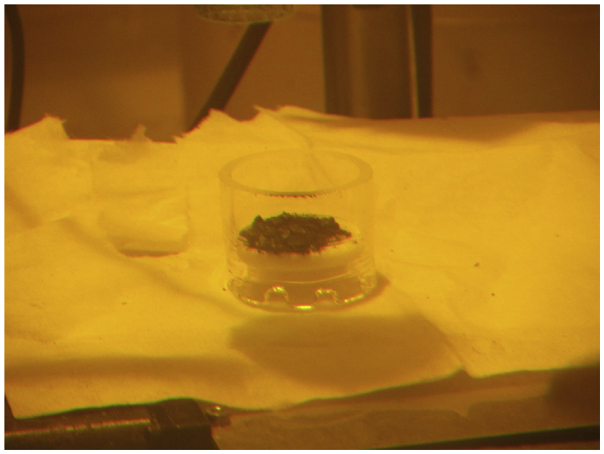

Fig. 4. SBS 1108 fuel fragments (grain size varying from 0.1 to 15.5 mm, average of 1.7 mm).

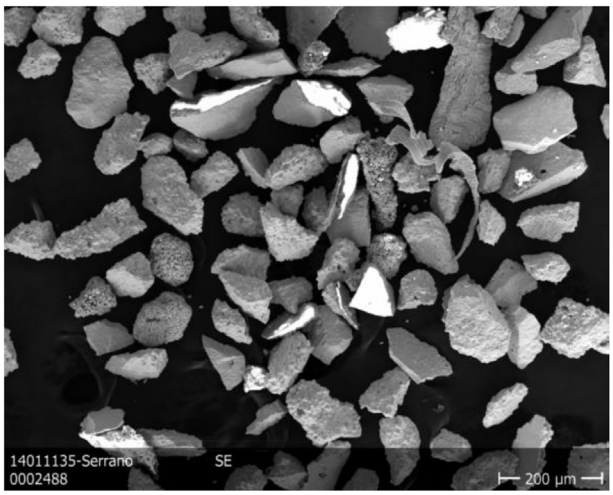

Fig. 5. Fuel powder from the outer zone of the pellet (fuel BWR54).

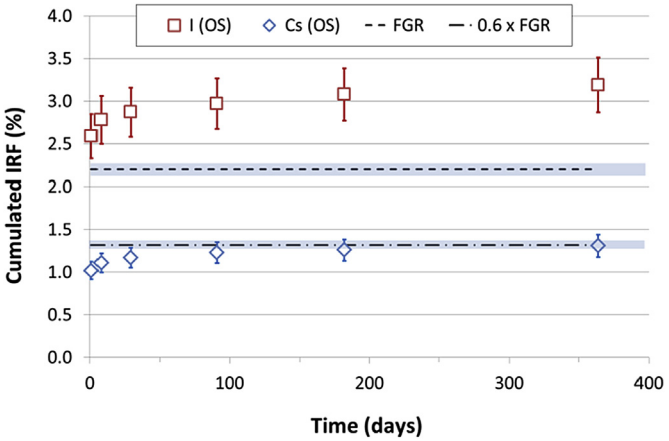

Fig. 6. Cumulated IRF (%) of cesium and iodine released from open segments (OS) of **PWR fuel VG81** as a function of time, with 95% confidence interval. The dotted lines show the Fission Gas Release (FGR) given by the operator and 0.6 × FGR, respectively. FRG for this fuel was 2.2 ± 0.07%. The 95% confidence interval for the FGR and 0.6 × FGR is shown by the shaded area along the dotted lines.

for a specific nuclide the fraction of the inventory in the solid sample released to the aqueous leaching solution at a given sampling time. The Instant Release Fraction (IRF) as defined here corresponds to the net release of all those elements/radionuclides that dissolve faster than the uranium oxide matrix, whatever their origin (gap, fissures and/or grain boundaries). In the tests under aerobic atmosphere, a measurable amount of UO_2 was also dissolved. Therefore the FIAP of the concerned radionuclide was corrected by subtracting the experimentally determined FIAP of uranium to calculate the IRF. In most cases, the effect of the correction is marginal, but in the case of fuel powders leached under aerobic conditions, the proportion of oxidative dissolution could not be neglected. The IRF for cesium and iodine will further be indicated as IRF(Cs) and IRF(I), respectively.

3.2. Evolution of the IRF with time

The leach data give information about the evolution of the IRF as a function of time and allow identifying the different regions within a (clad) pellet from which the released nuclides originate. This information can be derived by comparing data obtained on the same fuel but from differently prepared samples, e.g. clad fuel segments (S) vs. opened fuel segments (OS). The cumulative IRF for cesium and iodine as a function of time, as well as the FGR into the plenum (and also during the leaching in the case of the experiments by KIT) are plotted in Figs. 6–18. These graphs also show reference lines at 0.6 × FGR, corresponding to the expected cesium release. The background for this assumption is given in section 3.4.1. The maximum cumulative IRF values are given in Table 3. For some tests presented here, the iodine measurements were not reliable for the longer test durations. These long term data are not shown.

Figs. 6–18 show some different trends for PWR and BWR fuels. For the PWR samples (Figs. 6–10), the IRF(I) is in general significantly larger than IRF(Cs), and IRF(I) tends to exceed the FGR as provided by the utilities. For most BWR samples (Figs. 12–18), the difference between IRF(I) and IRF(Cs) is relatively small, and IRF(Cs) appears to be larger than IRF(I), while IRF(I) tends to be lower than FGR. These observations are in agreement with earlier publications [17,21].

All curves in Figs. 6–18 show gradually decreasing release rates, indicating fast depletion of soluble nuclides residing in the most accessible structures (gap, cracks, etc.), followed by slower release from less accessible features, typically grain boundaries. In many cases, the rates determined at the end of the experiments are very low, suggesting almost complete depletion of the soluble segregated elements at the accessible locations. However, in some tests the long term rate was still significant, especially for open segments and fragments. Previous tests on high burn-up samples also showed significant residual release rates after one year of leaching (especially for iodine) [27].

The systematically decreasing slopes in Figs. 6–18 imply that the release rates of I and Cs decrease steadily with time. Figs. 19 and 20 shows on a logarithmic scale all fractional dissolution rates for Cs and I from the leach tests of FIRST-Nuclides, expressed as inventory fraction per day (not in %). The fractional release rates of Cs and I for the damaged and leaking VVER fuels [40] are also included. They fit well with the rate evolution observed for the leach tests. Figs. 21 and 22 show the release rate for only the clad fuel segments, compared with a fitted equation described hereunder. In the log-log diagrams of Figs. 19–22, the decrease of the dissolution rates is recognizable as a linear trend. The relation between fractional

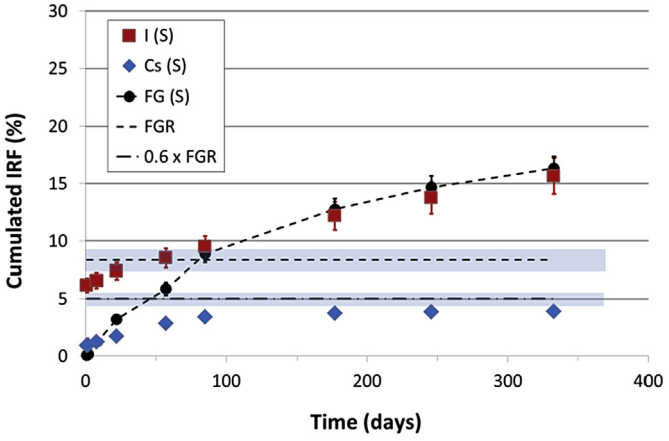

Fig. 7. Cumulated IRF (%) of cesium, iodine and fission gases (FG) released from clad fuel segments (S) of **PWR fuel SBS1108** as a function of time, with 95% confidence interval. When not visible, the error bars are hidden by the symbols. The dotted lines show the Fission Gas Release (FGR) given by the operator and 0.6 × FGR, respectively. FRG for this fuel was 8.34 ± 0.91%. The 95% confidence interval for the FGR and 0.6 × FGR is shown by the shaded area along the dotted lines.

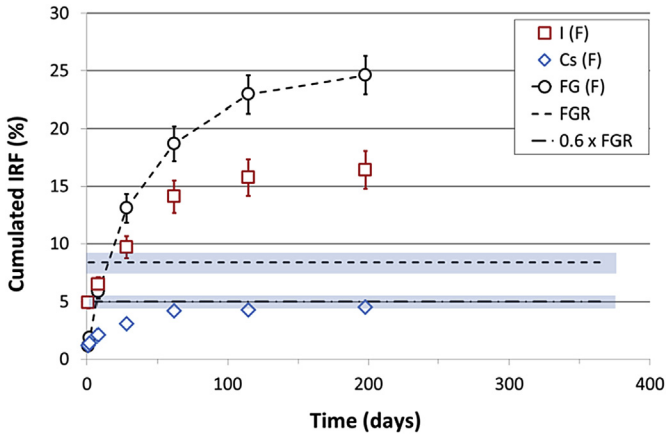

Fig. 8. Cumulated IRF (%) of cesium, iodine and fission gases (FG) released from fuel fragments (F) of **PWR fuel SBS1108** as a function of time, with 95% confidence interval. The dotted lines show the Fission Gas Release (FGR) given by the operator and 0.6 × FGR, respectively. FRG for this fuel was 8.34 ± 0.91%. The 95% confidence interval for the FGR and 0.6 × FGR is shown by the shaded area along the dotted lines.

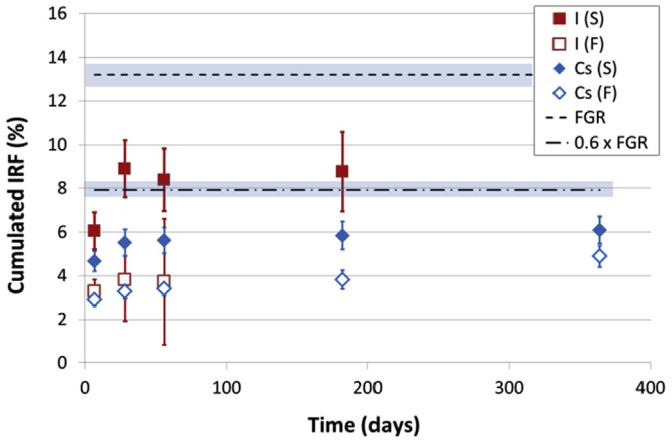

Fig. 9. Cumulated IRF (%) of cesium and iodine released from clad fuel segments (S) and fuel fragments (F) of **PWR fuel KKG-UO_2** as a function of time, with 95% confidence interval. The dotted lines show the Fission Gas Release (FGR) given by the operator and 0.6 × FGR, respectively. FRG for this fuel was 13.2 ± 0.5%. The 95% confidence interval for the FGR and 0.6 × FGR is shown by the shaded area along the dotted lines.

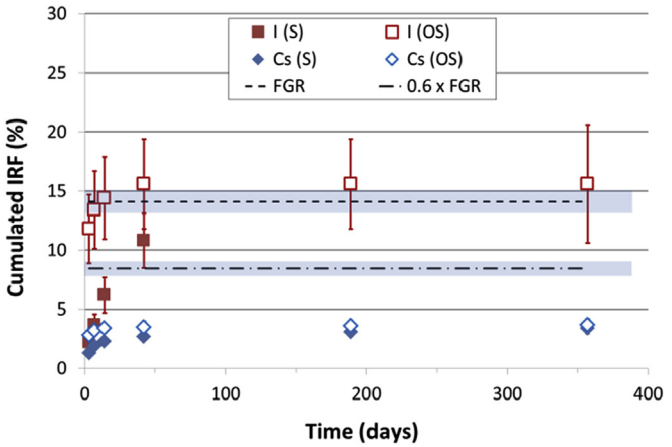

Fig. 10. Cumulated IRF (%) of cesium and iodine released from clad fuel segments (S) and open fuel segments (OS) of **PWR fuel D05** as a function of time, with 95% confidence interval. When not visible, the error bars are hidden by the symbols. The dotted lines show the Fission Gas Release (FGR) given by the operator and 0.6 × FGR, respectively. FRG for this fuel was 14.1 ± 0.9%. The 95% confidence interval for the FGR and 0.6 × FGR is shown by the shaded area along the dotted lines.

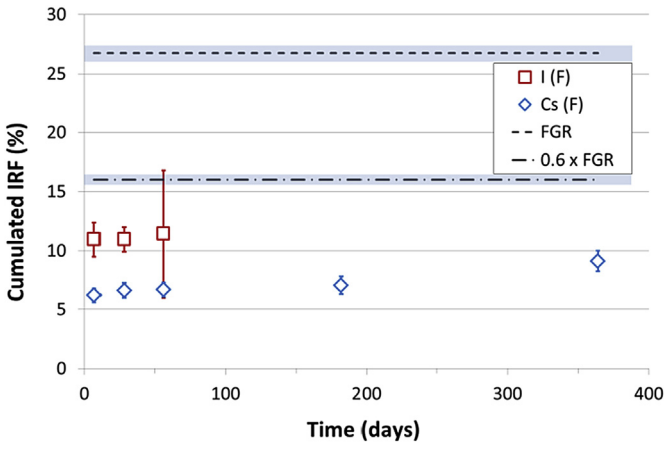

Fig. 11. Cumulated IRF (%) of Cs and I released from fuel fragments (F) of **PWR fuel KKG-MOX** as a function of time, with 95% confidence interval. The dotted lines show the Fission Gas Release (FGR) given by the operator and 0.6 × FGR, respectively. FRG for this fuel was 26.7 ± 0.6%. The 95% confidence interval for the FGR and 0.6 × FGR is shown by the shaded area along the dotted lines.

release rate and time is thus approached by the following linear equation (1):

$$\log(Rate) = a - b \times \log(t) \quad (1)$$

where t stands for time (days) and a and b are the intercept and slope, respectively. The exponential form of eq. (1) is given by eq. (2), with $A = 10^a$:

$$Rate = A \times t^{-b} \quad (2)$$

The coefficients a and b were calculated by linear regression for the various test series (see inserts in Figs. 21 and 22). The factor A in eq. (2) represents the rate after 1 day of aqueous corrosion and thus represents the fast release from the most accessible structures. The factor -b has a negative sign, making clear that the release rate decreases non-linearly with time. The more negative it is, the faster the rate decreases. It can be interpreted as an indicator of the accessibility of the internal structures (grain boundaries, fissures).

An alternative equation (Rate = A × e^{-bt}) was tested as well, but it did not well reproduce the data.

For the fuel segments (Figs. 21 and 22), only the most accessible structures will contribute to the release. The initial release rate of iodine is clearly higher than the release rate of cesium (A is larger for iodine), suggesting the iodine is present in the more accessible structures. Similar fits were made for the release rates measured with open segments, powders and fragments (the graphs are not shown). As expected, the parameter b is more negative for the release of iodine from open segments and fragments, because the leached surfaces are more accessible. For the powders the release rate seems to decrease faster than suggested by the exponential equation, probably because of depletion of the radionuclide source.

Although the parameters in the proposed rate equation can thus be related to macroscopic properties of the fuel, it is still an empirical equation that is not applicable for very short durations (the rate becomes infinitely large for very short durations), and for very long durations.

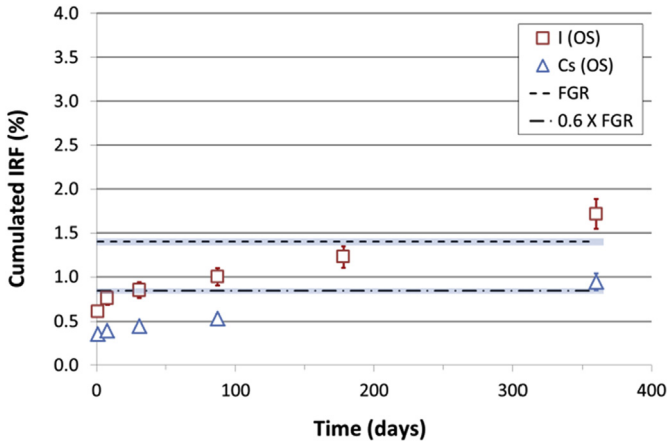

Fig. 12. Cumulated IRF (%) of Cs and I released from open segments (OS) of **BWR fuel C1** as a function of time, with 95% confidence interval. The dotted lines show the Fission Gas Release (FGR) given by the operator and 0.6 × FGR, respectively. FRG for this fuel was 1.4 ± 0.03%. The 95% confidence interval for the FGR and 0.6 × FGR is shown by the shaded area along the dotted lines.

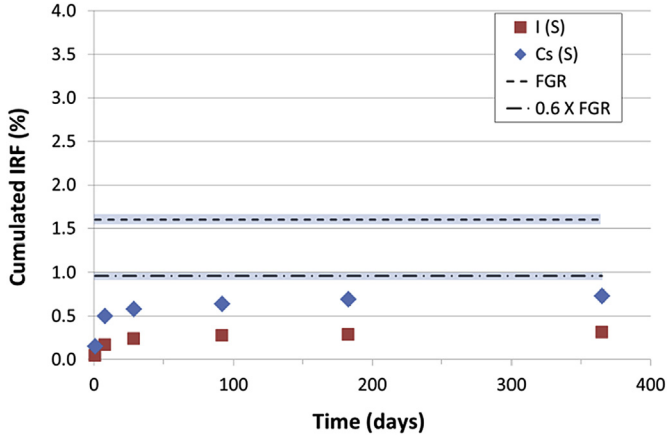

Fig. 13. Cumulated IRF (%) of Cs and I released from clad fuel segments (S) of **BWR fuel D07** as a function of time, with 95% confidence interval. When not visible, the error bars are hidden by the symbols. The dotted lines show the Fission Gas Release (FGR) given by the operator and 0.6 × FGR, respectively. FRG for this fuel was 1.6 ± 0.05%. The 95% confidence interval for the FGR and 0.6 × FGR is shown by the shaded area along the dotted lines.

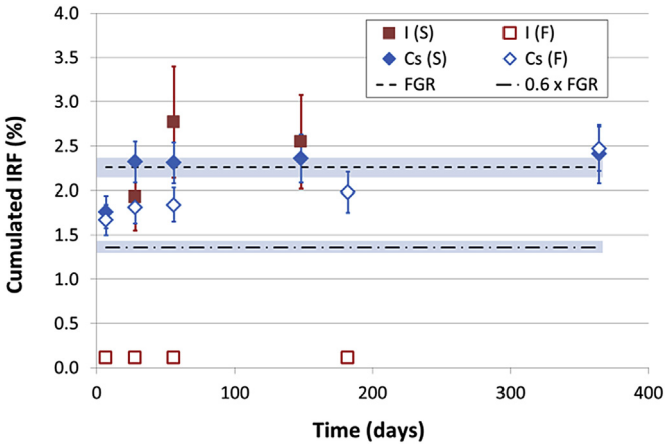

Fig. 14. Cumulated IRF (%) of Cs and I released from clad fuel segments (S) and fuel fragments (F) of **BWR fuel KKL-UO_2** as a function of time, with 95% confidence interval. The dotted lines show the Fission Gas Release (FGR) given by the operator and 0.6 × FGR, respectively. FRG for this fuel was 2.26 ± 0.1%. The 95% confidence interval for the FGR and 0.6 × FGR is shown by the shaded area along the dotted lines.

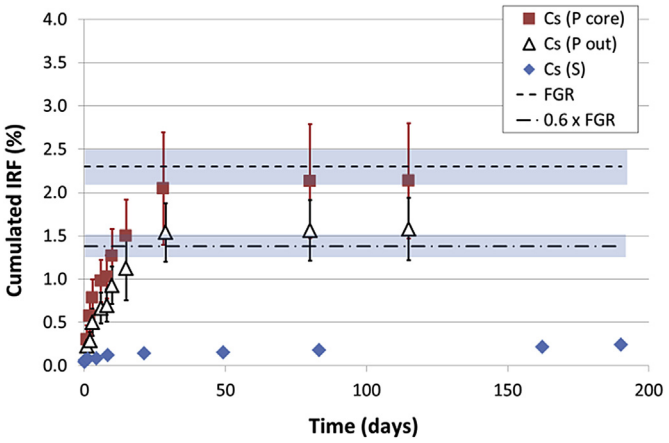

Fig. 15. Cumulated IRF (%) of Cs released from clad fuel segments (S) and fuel powder from the pellet core (P core) and pellet outer zone (P out) of **BWR fuel BWR42** as a function of time, with 95% confidence interval. When not visible, the error bars are hidden by the symbols. The dotted lines show the Fission Gas Release (FGR) given by the operator and 0.6 × FGR, respectively. FRG for this fuel was 2.3 ± 0.2%. The 95% confidence interval for the FGR and 0.6 × FGR is shown by the shaded area along the dotted lines.

3.3. *Effect of the sample preparation on the IRF*

By comparison of the leach data obtained from differently prepared SNF samples, the effects of different surface exposures on the IRF data can be estimated. Unfortunately, the limited number of experiments and the different SNF preparation procedures across the various laboratories proved to be a limiting factor in the interpretation of the results. In this section, we give a short account of the most salient observations arising from the comparison of leach data.

As expected, the release of iodine and cesium from open segment (OS) D05 was faster than for the segment that was not artificially opened (S) (Fig. 10), but this observation cannot be generalized because PWR fuel sample D05 is the only one where both types of samples were used.

The comparison of the release of iodine and cesium from fragments and from clad fuel segments (S) shows divergent results. Whereas both IRF(I) and IRF(Cs) increased faster in the case of SBS1108 fuel fragments compared to the leaching of the corresponding clad fuel segment (though reaching finally similar final IRF-values), the opposite behavior was observed for PWR fuel KKG-UO_2 and BWR fuel KKL-UO_2. In the latter experiments the cesium and iodine release from the clad fuel segments was faster and mostly larger than from the fuel fragments, possibly indicating dissolution of significant cesium and iodine inventories condensed on the inner surface of the cladding (see *General discussion*).

For the fuel powders (Figs. 15 and 18), IRF(Cs) was larger for the pellet core (P_{Core}) than for the pellet periphery (P_{Out}), and larger for the fuel powders than for the clad fuel segments (S), with one exception: for BWR54 (Fig. 18), IRF(Cs) was similar for P_{out} and the clad segment. Iodine was not measured for these samples.

3.4. *Comparison of IRF and FGR*

3.4.1. *Theoretical considerations*

Based on literature data, one can expect a similarity between the behavior of volatile fission products and fission gases. Coolant temperatures during reactor operation are in the range of 280 °C for

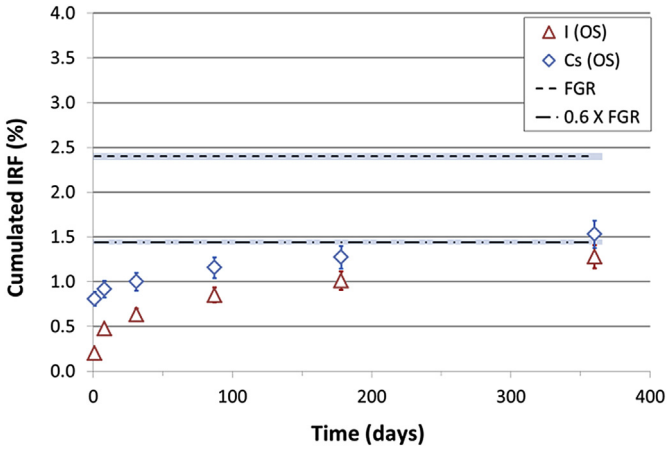

Fig. 16. Cumulated IRF (%) of Cs and I released from open segments (OS) of **BWR fuel 5A2** as a function of time, with 95% confidence interval. The dotted lines show the Fission Gas Release (FGR) given by the operator and 0.6 × FGR, respectively. FRG for this fuel was 2.4 ± 0.03%. The 95% confidence interval for the FGR and 0.6 × FGR is shown by the shaded area along the dotted lines.

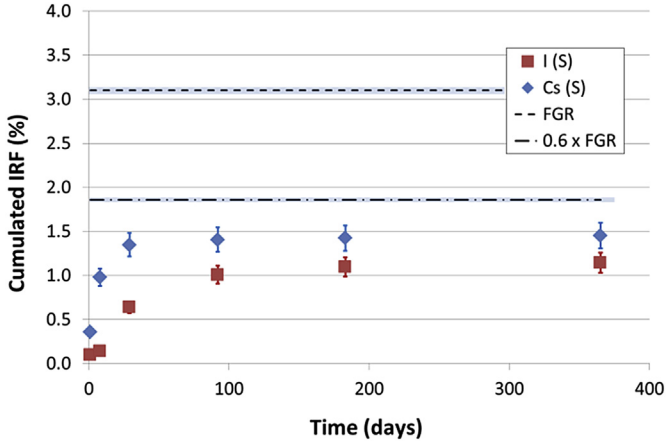

Fig. 17. Cumulated IRF (%) of Cs and I released from clad fuel segments (S) of **BWR fuel L04** as a function of time, with 95% confidence interval. When not visible, the confidence intervals are hidden by the symbols. The dotted lines show the Fission Gas Release (FGR) given by the operator and 0.6 × FGR, respectively. FRG for this fuel was 3.1 ± 0.03%. The 95% confidence interval for the FGR and 0.6 × FGR is shown by the shaded area along the dotted lines.

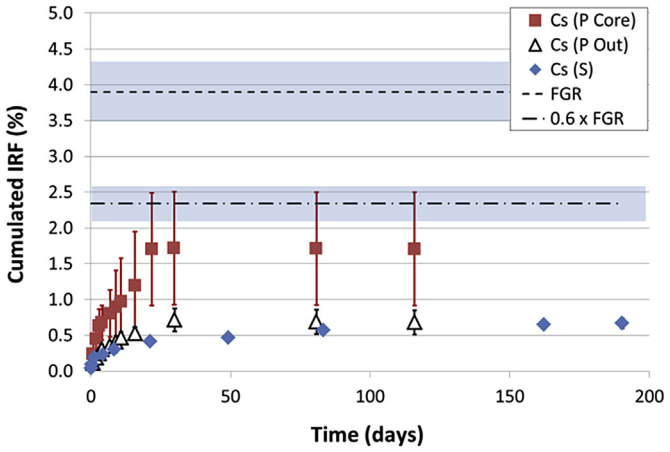

Fig. 18. Cumulated IRF (%) of Cs released from clad fuel segments (S) and fuel powder from the pellet core (P core) and pellet outer zone (P out) of **BWR fuel BWR54** as a function of time, with 95% confidence interval. When not visible, the error bars are hidden by the symbols. The dotted lines show the Fission Gas Release (FGR) given by the operator and 0.6 × FGR, respectively. FRG for this fuel was 3.9 ± 0.4%. The 95% confidence interval for the FGR and 0.6 × FGR is shown by the shaded area along the dotted lines.

BWR and up to 325 °C for PWR. During normal operating conditions LWR fuel experiences temperatures between ~1300 and 1500 K at the pellet centre and ~600–800 K at the rim [7,41]. The boiling point is 678.4 °C for cesium and 184.0 °C for iodine in their elemental form [42]. Already during the irradiation in the nuclear power plant, cesium tends to precipitate in colder regions of the rod. After cooling of the fuel, the fission gases remain in the gaseous state, whereas cesium and iodine precipitate. Although segregation may be considerable, the major part of the fission gas and volatiles is still retained in the fuel, especially in pores and on grain boundaries, where these species accumulate after diffusion through the UO_2 grains at the high temperatures during the irradiation [43]. Previous experiments have suggested similar diffusion rates for xenon and iodine under operating conditions due to the low boiling point of iodine [44]. On the other hand, Electron Probe Micro Analyses (EPMA) of local Cs/Xe ratios in spent fuel have suggested that cesium is less mobile than xenon in the fuel [45]. Up to a fractional, local Xe release of about 60%, the Cs/Xe ratio release is approximately 0.6. This ratio increases to reach unity at elevated releases of both elements. Assuming that grain boundary release dominates IRF(Cs), the ratio IRF (Cs)/FGR, should thus be approximately equal to 0.6 for fuels with a local FGR not exceeding 60%. The scatter in the data of [45] was significant, though. From the same set of data and using the fission gas release models integrated in the TRANSURANUS code, Lassmann et al. [45] derived a diffusion constant for Cs and expressed it relative to the Xe diffusion constant. The relative uncertainty on the ratio of these two diffusion constants was 300% at a 95% confidence interval. Because one considers iodine and xenon to diffuse identically, it should be expected that IRF(Cs) = 0.6 × IRF(I). As the diffusion constants depend strongly on the temperature, the FGR is influenced by the power ratings and power ramps. These operational parameters control the centreline temperature of the pellet [46]. Other factors that may affect the mobility of diffusing elements in the fuel are grain growth that may take place at high temperature in the centre of the fuel pellets [47], the degree of grain boundary interconnection [21], and fuel swelling causing closure of the gap between fuel and cladding.

The mobilization of iodine and cesium is probably controlled by the transport of water into the fuel and the subsequent transport of iodine and cesium along cracks, gaps and grain boundaries towards the bulk solution [48,49]. These processes are slower than the escape of over-pressurized fission gas during a puncturing test, or when the rods or opened to prepare fuel samples for the leach tests. The pressure of fission gases in the plenum and all connected voids is indeed high. For instance, the final pressure in the PWR fuel rod from which sample SBS 1108 was taken, was 37.155 ± 0.001 bar, compared to the initial He pressure of 21.5 bar [35]. For this reason, we expect that the IRF of iodine (or cesium) measured during a limited time in leach tests with clad fuel segments will often be lower than the FGR. The slopes of 1/1 for IRF(I)/FGR or 0.6 for IRF(Cs)/FGR mentioned in the previous paragraph would be rather theoretical maxima.

Fig. 23 shows a cross-section surface analysis of sample SBS1108. It shows that the initial gap was closed during reactor operation (as shown by fuel residues 'welded' to the white cladding material), but the fuel is cracked along the cladding. Fig. 24 shows a longitudinal section through a segment of the SBS1108 fuel rod,

Table 3
Overview of maximum cumulated IRF values (%) for cesium and iodine, and comparison with Fission Gas Release (FGR) for the fuels tested in FIRST-Nuclides. S = clad fuel segment, OS = open segment, F = fragment, C = core powder, O = out powder, na = not available. Burn-up is given in GWd.t_{HM}^{-1}.

Identification	VG81	SBS1108	KKG-UO_2	D05	KKG-MOX
Reactor	PWR	PWR	PWR	PWR	PWR
Burn-up	54.4	50.4	56.6	50.5	63
FGR (%)	2.2 ± 0.07	8.34 ± 0.91	13.2 ± 0.5	14.1 ± 0.9	26.7 ± 0.6
Sample type	OS	S/F	S/F	S/OS	F
IRF (Cs) (%)	1.3 ± 0.13	3.9 ± 0.4/4.5 ± 0.4	6.1 ± 0.6/4.9 ± 0.5	3.4 ± 0.5/3.7 ± 0.5	9.1 ± 0.9
IRF (I) (%)	3.2 ± 0.32	15.7 ± 1.6/16.4 ± 1.6	8.9 ± 1.3/3.8 ± 1.9	10.8 ± 2.3/15.6 ± 3.8	11.4 ± 5.4

Identification	C1	D07	KKL-UO_2	BWR42	5A2	L04	BWR54
Reactor	BWR	BWR	BWR	BWR	BWR	BWR	BWR
Burn-up	59.1	50.2	57.5	42	57.1	54.8	54
FGR (%)	1.4 ± 0.03	1.6 ± 0.05	2.26 ± 0.1	2.3 ± 0.2	2.4 ± 0.03	3.1 ± 0.03	3.9 ± 0.4
Sample type	OS	S	S/F	C/O/S	OS	S	C/O/S
IRF (Cs) (%)	0.94 ± 0.09	0.73 ± 0.07	2.4 ± 0.3/2.5 ± 0.25	2.1 ± 0.07/1.6 ± 0.36/0.24 ± 0.04	1.5 ± 0.15	1.5 ± 0.15	1.7 ± 0.8/0.68 ± 0.17/0.67 ± 0.07
IRF (I) (%)	1.7 ± 0.17	0.31 ± 0.03	2.8/0.11	na	1.3 ± 0.13	1.1 ± 0.11	na

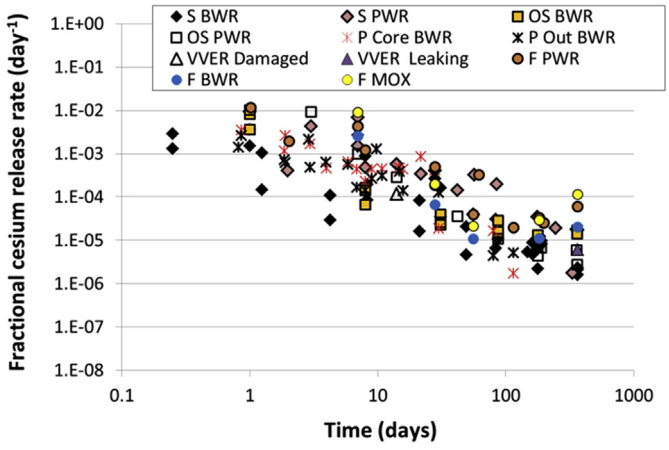

Fig. 19. Fractional release rates of cesium (day^{-1}) for all leach tests of FIRST-Nuclides as a function of time (S = clad fuel Segment, OS = Opened Segment, F = Fragment, P = Powder from the core or outer zone of the pellets, data for the damaged and leaking VVER fuel are also included).

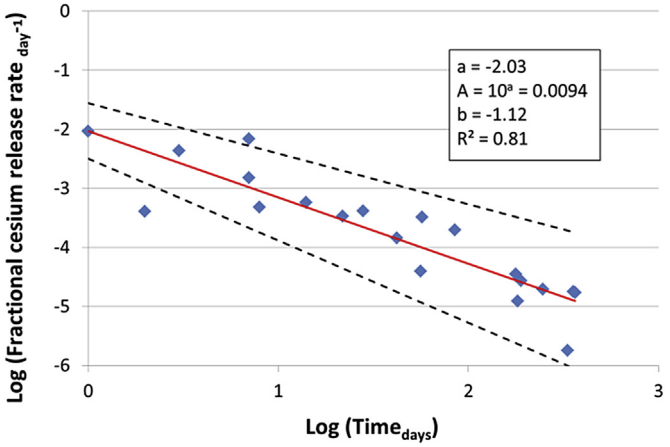

Fig. 21. Logarithm of the fractional release rates of cesium (day^{-1}) for the leach tests with clad PWR fuel segments (S) of FIRST-Nuclides, as a function of the logarithm of the test duration (days), showing the fit with equation (1) $Log\ (Rate) = a - b \times \log\ (t)$) for the given parameters a (and A from eq. (2)) and b, and the 95% confidence interval.

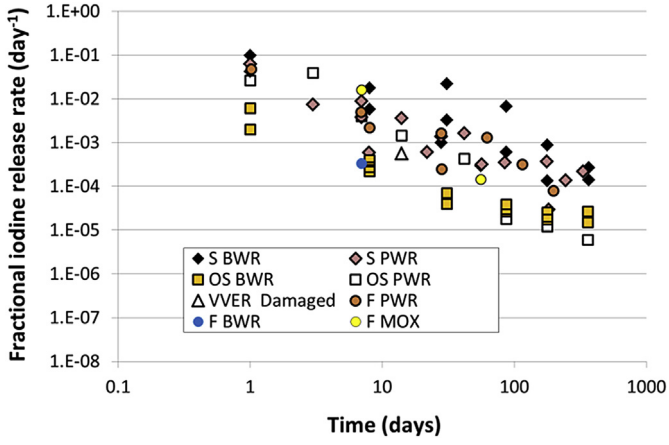

Fig. 20. Fractional release rates of iodine (day^{-1}) for all leach tests of FIRST-Nuclides as a function of time (S = clad fuel Segment, OS = Opened Segment, F = Fragment, data for the damaged and leaking VVER fuel are also included).

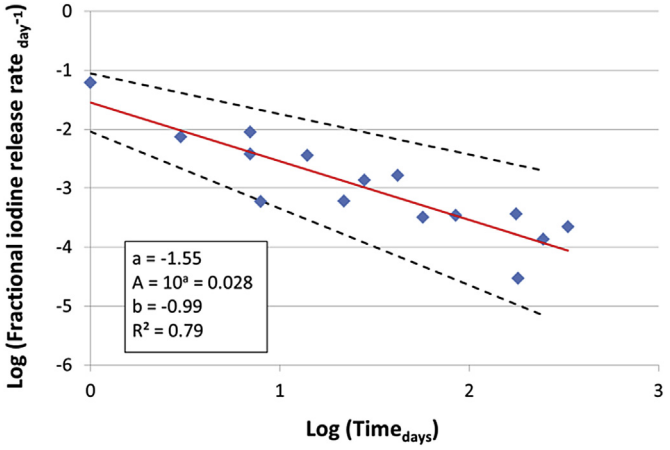

Fig. 22. Logarithm of the fractional release rates of iodine (day^{-1}) for the leach tests with clad PWR fuel Segments (S) of FIRST-Nuclides, as a function of the logarithm of the test duration (days), showing the fit with equation (1) $Log\ (Rate) = a - b \times \log\ (t)$) for the given parameters a (and A from eq. (2)) and b, and the 95% confidence interval.

revealing the cracked structure of the irradiated fuel pellet as well as two inter-pellet gaps. Cracks and gaps provide pathways for transport towards the fuel/cladding gap. Most cracks are narrow (≤0.1 mm). These cracks are expected to be saturated with water relatively quickly, within days or a few tens of days, depending on the exact crack width. After saturation with water, radionuclides will desorb and diffuse as dissolved species towards the external solution [48]. Fig. 25 (radial EPMA scan of sample D05 [50]) shows that the concentration of cesium in the fuel pellet increases very much near the gap for a fuel with high linear power rating. It is thus likely that the amount of leachable cesium is higher in the fissures close to the gap than in the central region. The same can be assumed for iodine.

3.4.2. Application to the leach tests

These considerations can now be used to interpret the leach results shown in Figs. 6–18. These graphs also include reference lines for FGR and 0.6 × FGR, corresponding to the theoretical diffusion behavior of iodine and cesium, respectively. The graphs show samples for which the cumulated IRF(I) and/or IRF(Cs) approach closely the reference lines, but for other samples the IRF seems to stabilize at much lower values. Finally, for some samples the reference lines are clearly exceeded. This is illustrated more specifically in Figs. 26–29, which show the maximum cumulated fast releases as a function of FGR for all leach tests of FIRST-Nuclides and comparable data from literature [21,27], together with the reference lines corresponding to IRF = FGR and IRF = 0.6 × FGR. The graphs also show lines corresponding to a 50% deviation from the reference lines (reference value ± 0.5 × reference value). Fast releases that fall in between these lines thus deviate by less than 50% from the theoretical behavior expected from the assumptions made in section 3.4.1. For IRF(Cs), the 50% range is close to the 95% confidence level range given by Lassmann [45].

3.4.2.1. Iodine release. In agreement with the above considerations, for most tests with clad fuel segments, where transport from the grain boundaries to the leachate is thought to be retarded by the limited accessibility, the IRF(I) was below the FGR. For the KKL-UO_2 (S) sample (Fig. 14), IRF(I) coincided with the FGR, suggesting either a very open structure (like in Figs. 23 and 24) or a higher local FGR than the reported rod average value of 2.26%. The latter explanation was brought forward to explain previous experiments performed with Ringhals 3 PWR samples with a burn-up of 58.2 GWd/t_{HM}, which also showed a much higher I release than the FGR [21]. For the SBS1108 segment, IRF(I) also evolves quickly to the average rod FGR, but continues to increase afterwards (Fig. 7).

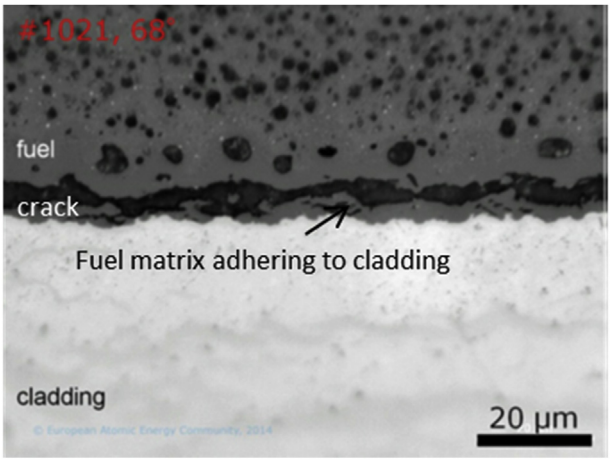

Fig. 23. Optical microscopy cross-sectional micrograph showing the fuel pellet/cladding interface of fuel SBS1108. The presence of a crack between the pellet and the cladding after irradiation is shown.

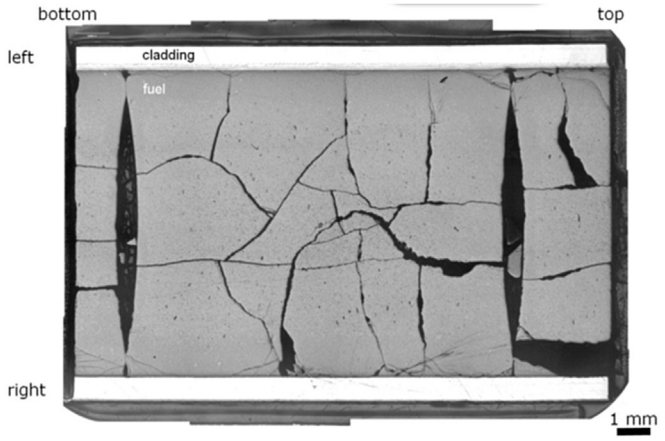

Fig. 24. Optical microscopy macrograph of a longitudinal section of the SBS1108 fuel rod.

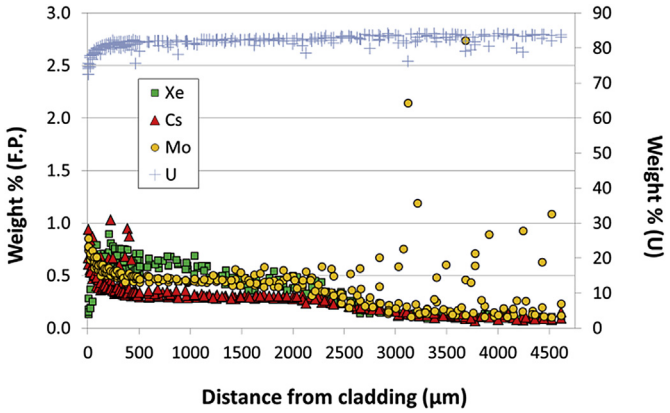

Fig. 25. Radial concentration profile of Xe, Cs, Mo and U by EPMA scan of sample D05 [50].

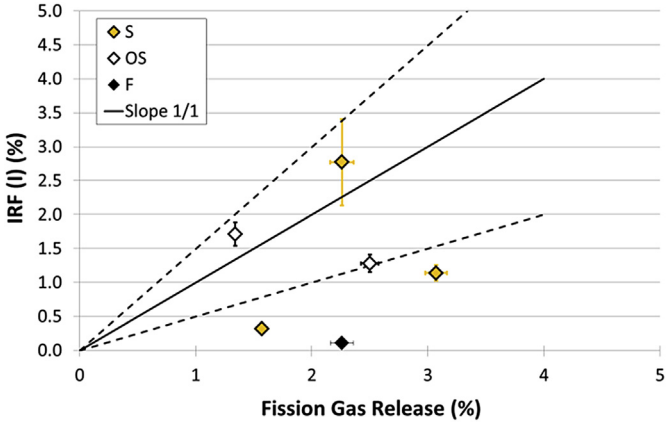

Fig. 26. Maximum cumulated IRF of iodine (%) as a function of Fission Gas Release (%) for the BWR samples, with 95% confidence intervals; when not visible, the error bars are hidden by the symbols; the dotted lines indicate IRF deviations of ±50% from the ideal slope 1/1, shown as a solid line; Legend: S = clad fuel Segment, OS = Open Segment, F = Fragment.

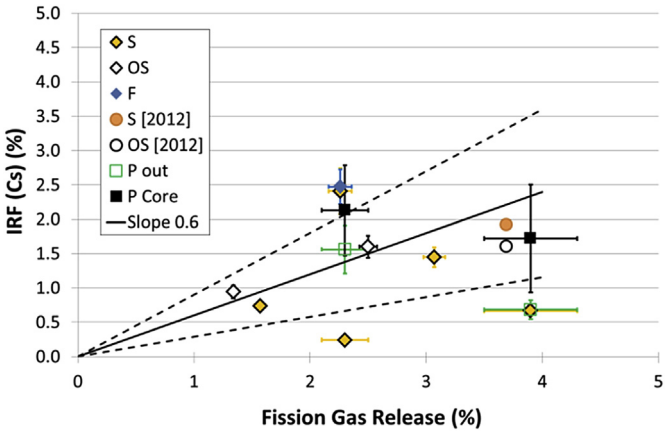

Fig. 27. Maximum cumulated IRF of cesium (%) as a function of Fission Gas Release (%) for the BWR samples, with 95% confidence intervals; when not visible, the error bars are hidden by the symbols; the dotted lines indicate IRF deviations of ±50% from the ideal slope 0.6, shown as a solid line; the data indicated as [2012] were taken from Johnson [21] and Ekeroth [27]; Legend: S = clad fuel Segment, OS = Open Segment, F = Fragment, P = Powder from the core or outer zone of the pellets.

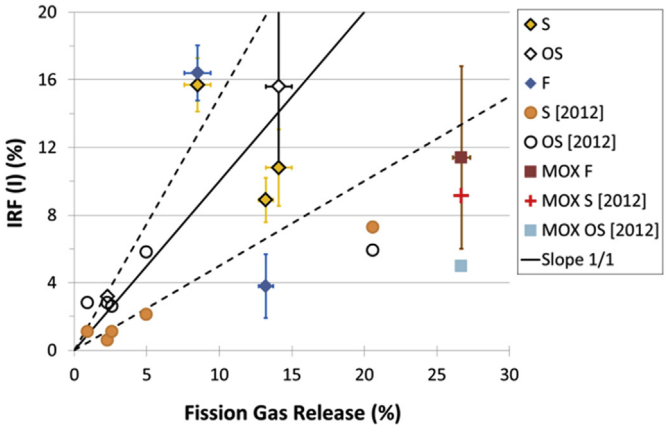

Fig. 28. Maximum cumulated IRF of iodine (%) as a function of Fission Gas Release (%) for the PWR samples, with 95% confidence intervals; the dotted lines indicate IRF deviations of ±50% from the ideal slope 1/1, shown as a solid line; the data indicated as [2012] were taken from Johnson [21] and Ekeroth [27]; the 95% confidence intervals are shown only for the data from FIRST-Nuclides; Legend: S = clad fuel Segment, OS = Open Segment, F = Fragment.

The fact that the IRF(I) from several segments under investigation was found at a level below the FGR suggests that the closed gap partially blocks the transport path and consequently the release of IRF nuclides. This interpretation is supported by previous observations with longer segments ('rodlets') [27]. Because of the limited accessibility of the gap, the ratio of the exposed fuel surface area/fuel mass will be lower when longer segments are used, thereby decreasing the IRF.

When the segments are opened, complete release of the leachable iodine is expected, as shown by sample D05 (Fig. 10). This confirms earlier results [21], where opening of the segments also led to an iodine release close to the FGR for PWR fuels with a burn-up of 61.4 GWd/t_U, 66.5 GWd/t_{HM} and 75.4 GWd/t_{HM}. In the open segment sample 5A2, IRF(I) remained lower than the FGR, but the release rate at the last test duration was still high (Fig. 16). The measured iodine release may be biased by heating of the sample when the cladding was axially cut [51], although iodine loss during the subsequent handling seems more likely. Johnson also reported one open fuel segment for which the iodine release was much lower than the in-reactor FGR (a PWR fuel of 64 GWd/t_{HM}) [21]. The

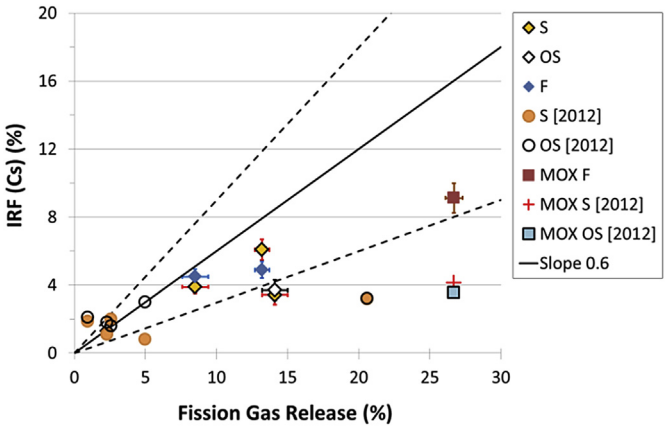

Fig. 29. Maximum cumulated IRF of cesium (%) as a function of Fission Gas Release for the PWR samples, with 95% confidence intervals; the dotted lines indicate IRF deviations of ±50% from the ideal slope 0.6, shown as a solid line; the data indicated as [2012] were taken from Johnson [21] and Ekeroth [27]; the 95% confidence intervals are shown only for the data from FIRST-Nuclides; Legend: S = clad fuel segment, OS = Open Segment, F = Fragment.

only OS sample (in FIRST-Nuclides) that was prepared without sawing, and thus without any heat generation, was sample D05.

For sample VG81 (Fig. 6) and SBS1108 (Fig. 7), IRF(I) was clearly higher than the FGR reported by the utilities. This might be due to an underestimation of the local FGR [21,27]. The FGR given for SBS1108 is, however, not unusual for the average linear power rating of the fuel, thus calling for another mechanism. Because fission gases and iodine are believed to have a similar mobility in the fuel during the reactor operation, the fraction of surface-precipitated iodine released via aqueous leaching should ideally be comparable to the in-reactor FGR determined e.g. by measurements of ^{85}Kr at the plenum of the rods [22]. When the fuel rod is punctured, the free fission gas in the plenum and other voids escapes immediately, but the condensed iodine remains at the surfaces. For the SBS1018 samples, the further release of fission gas was also measured during the leaching experiment, and it appeared to be very significant and correlated to iodine release. This suggests that, apart from a directly available fraction of surface-precipitated iodine, there is another fraction of iodine associated to fission gases in pores that becomes available only upon contact with the leachant. Figs. 7 and 8 show that the continuous fission gas release is faster and higher for the fragments than for the clad fuel segment. The origin of this iodine fraction is not clear, but it can still be considered as part of the instant release fraction.

The Cr/Al doped sample C1 (open segment) shows a cumulated IRF(I) after 1 year close to the FGR, but the iodine release rate is still high at the end of the test (Fig. 12). This can be compared with the results for fuel 5A2 (Fig. 16), which had a similar irradiation history, but was not doped. It appears that the FGR and IRF(Cs) is lower for fuel C1 than for fuel 5A2. This is indeed the expected behavior for this doped fuel, designed to have larger grain sizes, so that the diffusion distances required for fission products to reach the grain boundaries are increased. The release rate for iodine after 1 year is, however, clearly higher for C1 than for 5A2. This can probably be explained by the loss of iodine from the 5A2 sample during the experiment (e.g. during longitudinal cutting of the samples or during the initial sampling of the leaching solution). Additional experiments were performed, showing lower release rates for both cesium and iodine for doped fuel at the initial phase of the experiment, whereas the difference between doped and undoped was less pronounced at longer time scales [51], so the favorable effect of the doping seems to be only temporary. No general conclusion can

be drawn from this isolated test, so more IRF data on doped fuels are urgently needed.

In summary, we conclude that the differences in iodine release of closed and open segments can be explained relatively well by the accessibility of the fuel surface in the different types of samples. The few cases where IRF(I) was higher than the FGR cannot be explained and have to be investigated further. Some tests with UO_2 fuel fragments show very little iodine release (KKL-UO_2 (Fig. 14), KKG-UO_2 (Fig. 9)). This may be due to the sample preparation technique (see *General discussion*).

The test with KKG-MOX fragments (Fig. 11) yielded a cumulated IRF(I) of 11.5% after 56 days, which basically confirms earlier results on closed and open segments of the same fuel [21]. However, this value is still much lower than the FGR of 26.7%. Clearly, further leaching data are needed to understand instant release from MOX fuel and to reach robust conclusions.

Figs. 26 and 28 illustrate that the IRF(I) is varying, but only in exceptional cases higher than the FGR, in agreement with the theoretical considerations. The NIKUSI fuel SBS1108 is the main exception, due to the apparent continuous release of iodine and fission gases.

3.4.2.2. Cesium release. IRF(Cs) is lower than IRF(I) and FGR for the PWR samples and reaches approximately 0.6 × FGR (or is higher) for several samples, while for other samples IRF(Cs) levels off below this value (Figs. 6–18, 27, 29). On the other hand IRF(Cs) is clearly higher than IRF(I) for four BWR samples (D07(S) (Fig. 13), KKL-UO_2(F) (Figs. 14), 5A2(OS) (Fig. 16) and L04(S) (Fig. 17)). These samples are characterized by low linear power rating and FGR. Johnson also reported IRF(Cs) > IRF(I) for clad segments of PWR fuels with high burn-ups (58.2, 61.4 and 66.5 GWd/t_{HM}), low peak linear powers (200, 230 and 220 W cm^{-1}, respectively) and low FGR [21]. In agreement with the theoretical considerations, IRF(Cs) is only in exceptional cases significantly higher than 0.6 × FGR. Such cases are found only for a few fuel samples with low FGR (<3%), i.e. the BWR fuel KKL-UO_2 (S and F) (Fig. 14) and the BWR42 core powder (Fig. 15), and a previously investigated PWR for which the average FGR of 0.94% may underestimate the local FGR [21]. Fuel samples with remarkably low IRF(Cs) are D05 (S and OS) (Fig. 10) and some previously investigated fuels, i.e. a fuel with a FGR of 5% and a very high burn-up of 75.4 GWd/t_{HM}, and a PWR fuel with FGR 20.6% and a burn-up of 64 GWd/t_{HM} [21]. The IRF(Cs) for doped fuel C1 (Fig. 12) and standard fuel 5A2 (Fig. 16) approach very well the 0.6 × FGR reference line. The cesium release is thus lower for the doped fuel than for the standard fuel, although they had a similar irradiation history, as a result of the larger grain size of the doped fuel. The data for MOX fuel suggest that the cesium release is much lower than 0.6 × FGR, but the data base for MOX fuel is too limited to draw general conclusions.

3.4.2.3. IRF versus linear power rating. Because the linear power rating (LPR) determines the temperature in the fuel during operation, one can expect the IRF of iodine and cesium to be positively correlated to this parameter. For the BWR samples, no correlation is visible between the maximum cumulated IRF and the rod average LPR (Figs. 30 and 31). A variation of the rod average LPR between 143 W cm^{-1} and 217 W cm^{-1} does not lead to a clear increase of the IRF. In contrast, for the PWR samples (Figs. 32 and 33), the IRF depends much more on the rod average LPR. In the power rating range 136–321 W cm^{-1}, IRF(I) varies from 1 to 16%. A plot of the combined BWR and PWR data (the BWR data are shown as light grey symbols in Figs. 32 and 33) suggests that independent of the reactor type, BWR or PWR, there is no clear effect below 200 W cm^{-1}, but an overall positive correlation at higher LPR. A plot of the FGR as a function of rod average LPR shows a similar trend (Fig. 34). The scatter of the data in Figs. 32 and 33 is still significant, possibly due to variable sample preparations: IRF from segments with cladding, open segments, fragments, and powders are plotted together, although they have different exposed surface areas and different initial inventories. This is especially the case for the BWR fuel powders, which have a specific surface area that is much higher than for the opened or closed segments, but no gap inventory. Moreover, the plots of Figs. 32 and 33 combine rod average LPR for the samples of FIRST-Nuclides, with peak LPR for the fuels from previous work [21,27] (the latter papers only mention peak LPR). Nevertheless, the correlation quality is certainly better than for the IRF-FGR graphs of Figs. 26–29 and than for plots of IRF as a function of the burn-up, which show no correlation at all and are therefore not shown in this paper. These results confirm that the linear power rating can be used as a promising alternative estimator for the IRF of cesium and iodine, although a more detailed study will be necessary to consolidate the correlation between IRF and LPR (see section *General discussion*).

4. General discussion

During the last decades, fast release was often related to fuel burn-up, to obtain estimates for performance assessment. The acquisition of more data on high burn-up fuels showed a growing evidence that fission gas release and fast release correlate better with the linear power rating (LPR) of the fuel than with the burn-up [21]. The data gathered in the framework of FIRST-Nuclides provide further convincing evidence in this direction. Figs. 32 and 33 show that there is indeed a trend for a positive correlation between the IRF of cesium and iodine with LPR higher than 200 W cm^{-1}. Hence, LPR appears to be a more relevant operational parameter to predict the FGR and fast release than the burn-up, for fuels with sufficiently high LPR. This can be explained by the fact that LPR, rather than burn-up, correlates with the temperature of the fuel pellet in the reactor. The higher the fuel temperature during reactor operation, the higher the FGR and faster the diffusion of volatile fission products. In contrast, high burn-ups may be reached through a large number of burning cycles at low power and are therefore not necessarily correlated with high operational temperatures. The data in Figs. 30–33 still show significant scatter, which may partly be due to different sample preparations and test durations, and to the fact that rod average LPR values (tests of FIRST-Nuclides) are plotted together with maximum LPR values (tests from Refs. [21] and [27]). Average and maximum LPR can be very different,

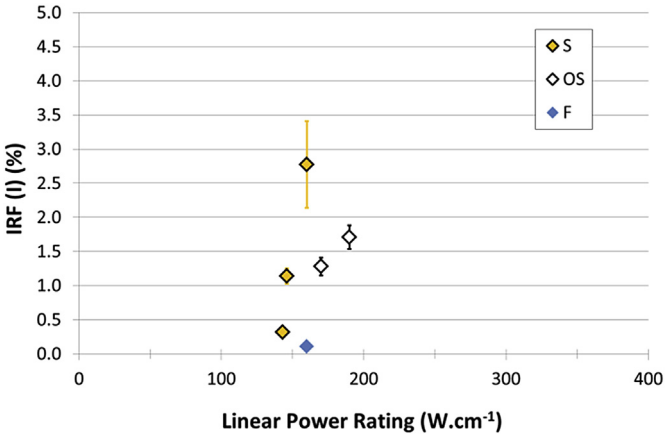

Fig. 30. Maximum cumulated IRF of iodine (%) as a function of the rod average linear power rating (W.cm^{-1}) for BWR fuels, with 95% confidence interval; when not visible, the error bars are hidden by the symbols; Legend: S = clad fuel segment, OS = open segment, F = fragment.

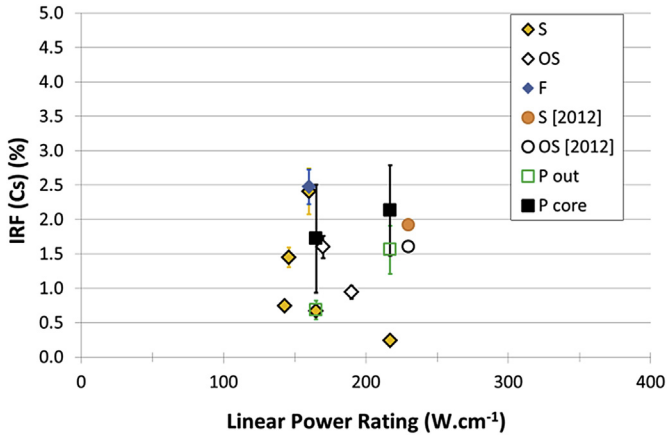

Fig. 31. Maximum cumulated IRF of cesium (%) as a function of the rod average linear power rating ($W.cm^{-1}$) for BWR fuels, with 95% confidence interval; the data indicated as [2012] were taken from Johnson [21] and Ekeroth [27], and represent peak linear power rating values; the 95% confidence intervals are shown only for the data from FIRST-Nuclides; when not visible, they are hidden by the symbols; Legend: S = clad fuel segment, OS = open segment, F = fragment, P = powder from the core or outer zone of the pellets.

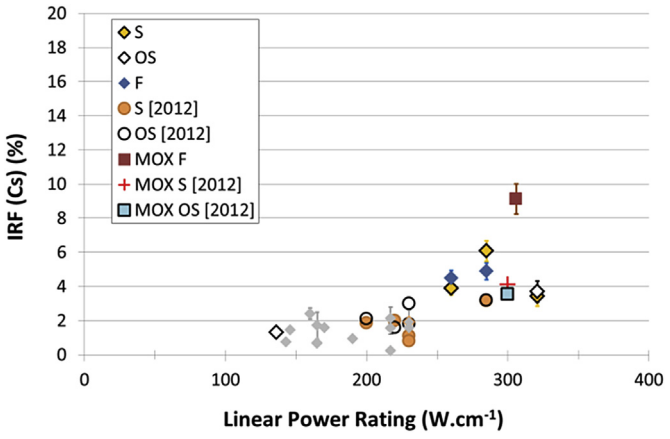

Fig. 33. Maximum cumulated IRF of c (%) as a function of rod linear power rating ($W.cm^{-1}$) for PWR and BWR fuels (in grey, same data as in Fig. 30), with 95% confidence interval; the data indicated as [2012], taken from Johnson [21] and Ekeroth [27], represent peak linear power rating values, whereas all other data are rod average values; 95% confidence intervals are shown only for the data from FIRST-Nuclides and when they exceed symbol size. Legend: S = clad fuel segment, OS = open segment, F = fragment.

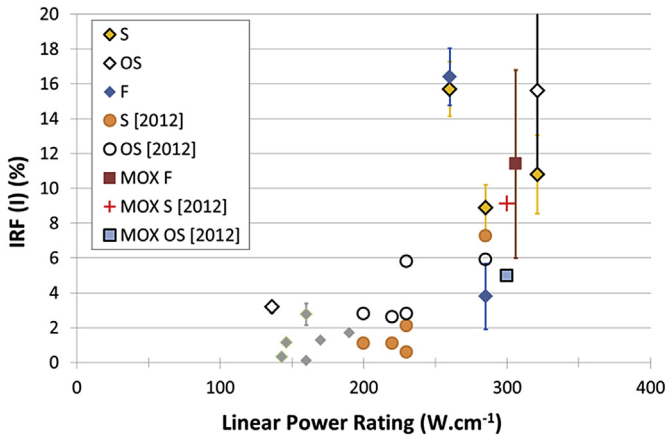

Fig. 32. Maximum cumulated IRF of iodine (%) as a function of rod linear power rating ($W.cm^{-1}$) for PWR and BWR fuels (in grey, same data as in Fig. 30), with 95% confidence interval; the data indicated as [2012], taken from Johnson [21] and Ekeroth [27], represent peak linear power rating values, whereas all other data are rod average values; 95% confidence intervals are shown only for the data from FIRST-Nuclides and when they exceed symbol size. Legend: S = clad fuel segment, OS = open segment, F = fragment.

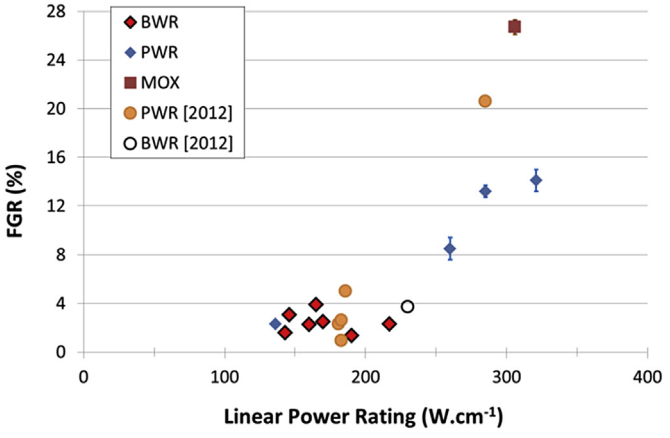

Fig. 34. FGR (%) as a function of rod average linear power rating ($W.cm^{-1}$) for PWR and BWR fuels; the data indicated as [2012] were taken from Johnson [21] and Ekeroth [27] and represent peak linear power rating values; the 95% confidence intervals are shown only for the data from FIRST-Nuclides; for most fuels, they are hidden by the symbol.

because of the variations in LPR during the irradiation. This leads to important variations in the centreline temperature, as illustrated for fuels BWR42 and BWR54 in Fig. 35, and hence a different mobility of the volatile fission products. In future investigations, it should be tested whether a fine-tuning of the LPR as a parameter would help in improving the correlation, but this can only be done if the complete linear power data are available from the nuclear power plant owners.

The gas measurements during the leach test with fuel SBS1108 have shown that FGR continues during the leaching of the fuel and that this is associated with fast iodine release (Figs. 7 and 8). For no other fuel tested in FIRST-Nuclides, such a high iodine release was observed, although a similarly high iodine release has been observed before [27]. The behavior of SBS1108 might be due to the fact that the SBS1108 test samples were cut at the pellet-pellet interface, where cesium and iodine tend to concentrate during reactor operation, whereas the other samples were cut in the middle of the pellets, or to the smaller grain size in this fuel (produced with the NIKUSI process). We do not think that the high continued FGR can be due to the reducing test conditions for fuel SBS1108 (all other experiments were conducted in oxidizing conditions), because the fast release of cesium and iodine is not expected to depend on redox conditions. In aqueous solutions, cesium is only stable in the +I state and does not precipitate. In the case of iodine, several oxidation states are conceivable, but all of them lead to soluble or volatile species. The fact that the conditions were effectively reducing is confirmed by the low measured technetium concentrations (10^{-12}–10^{-14} M or below detection limit). Tests with cracked TRISO particles (with very high burn-up of 95.57 GWd/t_{HM}), performed for FIRST-Nuclides, also showed an apparently unfavorable effect of the reducing atmosphere on the cesium leaching [52,53]. In these experiments, 9% of the cesium was leached under reducing atmosphere, compared to 5% under air. The possible effect of the redox conditions on the fast release is clearly not yet sufficiently understood.

Figs. 26–29 show that the fast release of iodine and cesium can

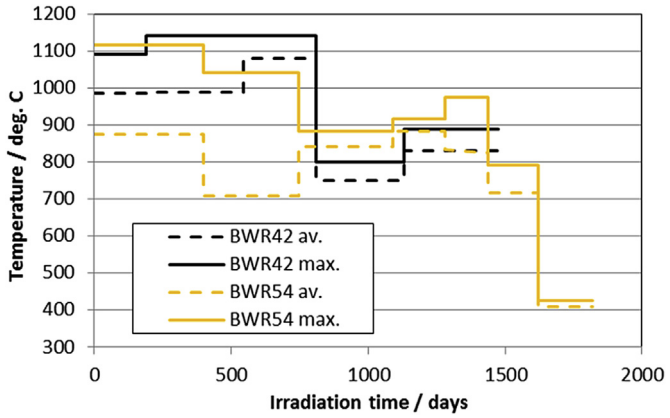

Fig. 35. Calculated average and maximum centreline temperatures of BWR42 and BWR54 as a function of irradiation time. The temperature was calculated with the TRANSURANUS code for fuel BWR54, and with a code provided by the fuel vendor for fuel BWR42.

vary, but IRF values higher than FGR (for I) or than 0.6 × FGR (for Cs) are exceptional, confirming earlier findings [21,27]. To explain the variation, a detailed interpretation of each separate test should be performed, which is out of the scope of this paper. Low IRF values for iodine may be due to loss of iodine during the analyses, leading sometimes to an artificial decrease of the cumulated IRF, or to the fuel sample treatment (the heating during the axial cutting). A low cumulated IRF may also be the consequence of a test duration that was too short. A continuation of the leaching for some years might in several cases significantly increase the IRF. On the other hand, the few IRF values exceeding FGR may be explained by underestimation of the latter parameter (differences in local and rod-averaged FGR).

Overall, the IRF of cesium or iodine are relatively coherent, considering the different sample preparations (segments, open segments, fragments and powders). IRF (I) and IRF (Cs) follow the trend: $S \leq OS$. For the powders only IRF(Cs) was measured, and this follows the trend: $S \leq P_{Out} < P_{Core}$. The tests with fragments gave varying IRF results, with $F > S$ or $F \leq S$.

In the tests where the cladding is opened and exposed to the leachant together with the fuel fragments (OS), the exposed specific surface area is larger than for the clad fuel segments, and the transport towards the bulk leachant is not delayed by narrow fissures. The release is thus faster for an open segment than for an assembled segment (see results for D05, Fig. 10), in agreement with previous work [21].

Although the segments have a relatively small exposed specific surface area, the presence of the cladding and of the adhering fuel with high cesium and iodine concentrations (Figs. 23 and 25) can lead to the release of an additional inventory (not present in the other sample types), if these surfaces are accessible. The closure of the gap due to fuel swelling at high burn-up does not appear to stop the release of mobile nuclides, but it slows it down, as shown by the tests with fuel D05. Fig. 23 shows that the swelling of fuel SBS1108 effectively fills up the gap and that the fuel in direct contact with the cladding is tightly bound, but it also shows a fissure with a width of about 2 μm parallel to the cladding at few μm distance inward from the fuel-cladding interface. Similar observations were made for fuel D05. It is likely that transport is not taking place in the original gap (which is closed), but in the parallel fissures, very close to the original gap.

The exposed specific surface area of powder samples (fuel BWR42 (Fig. 15) and BWR54 (Fig. 18)) is very large, and much of this surface area consists of accessible grain boundaries, that may have been opened by the crushing procedure. This increases the amount of readily leachable cesium and iodine compared to the other sample types. The increase in water-accessible surface area seems to compensate or even overcompensate for the absence of the fraction adhered to the cladding. A similar observation was done in a previous short term experiment (10–30 days) with PWR fuel of 75.4 MWd/t_{HM}, where the IRF(Cs) increased faster for the powder than for the segment, but quickly evolved to the released fraction for the opened segment [27]. When the cesium release from the BWR42 and BWR54 fuel is normalized with regard to the surface area, which is two orders of magnitude higher for the fuel powders than for the fuel segments, the resulting IRF(Cs) per unit of exposed surface area is an order of magnitude lower for the powders than for the segments. This suggests that the cesium in the internal grain boundaries from both the core and outer region of the fuel is less leachable than the cesium close to the gap. The results for the BWR42 and BWR52 powders further show that the cesium present in the core is more easily dissolved than the cesium present in the outer region, as observed already in Ref. [54] for a PWR fuel with a burn-up of 48GWd/t_{HM}. Similar tests were performed previously using a PWR fuel with a burn-up of 60 GWd/t_{HM} and a FGR of 15% (i.e. much higher than for the present BWR fuels) [55]. They showed that the initial cesium dissolution rate was higher for the periphery than for the centre, but in the longer term the release rate would be presumably lower, because the recrystallisation process in the high burn-up structure would reduce water permeability (in spite of its higher porosity). This interpretation is based on the availability of distinct data for the initial release, representing directly accessible sites, and the longer term release, presumed to be controlled by water diffusion in the grain boundaries. A similar interpretation may be applied to the analogous powder tests of FIRST-Nuclides. Specific surface analyses on leached samples that give more information about the mechanism of transport in the grain boundaries are not available for the here discussed leach tests in FIRST-Nuclides. So the mechanism of this transport is still unclear. Transport might take place via connected tunnels at the grain edges, and chemical attack may open closed grain boundaries. An additional dissolution mechanism may be provided by evaporation/condensation, which is much more penetrating than wetting by a liquid phase. It remains unclear whether these mechanisms effectively played a role for the investigated samples.

For the (mm size) fuel fragments of fuels SBS1108 (Fig. 8), KKG-UO_2 (Fig. 9), KKG-MOX (Fig. 11), KKL-UO_2 (Fig. 14), we can expect a relatively fast and high IRF, compared to the (closed) segments, because they have a relatively high accessible surface area. Moreover, the preparation of the fragments might create an extra open porosity which will be immediately available for leaching. This can explain why IRF(I) and IRF(Cs) increased faster for the SBS1108 fragments than for the segment (Figs. 7 and 8). At the end of the experiments, however, the IRF was similar for both types of samples, because the release from the extra open porosity stops, while in the case of the segment the diffusion of cesium and iodine coming from the less accessible regions (internal cracks/fractures and grain boundaries) towards the bulk solution goes on. The KKL-UO_2 fragments (Fig. 14) showed, however, a slower release compared to the segment, although the final IRF(Cs) was the same for both sample types. For fuel KKG-UO_2 (Fig. 9), IRF(Cs) for the fragment sample was lower than for the segment during the entire experiment. Both for KKL-UO_2 and KKG-UO_2, IRF(I) was very low for the fragments. This suggests that a considerable part of the segregated iodine and cesium inventories resided in the fuel/sheath gap or in the porous oxidized layer at the inner side of the cladding. If such regions are readily accessible to water, they would account for the difference observed between release from clad segments and fragmented fuel samples. This gap inventory is obviously not

present in the fuel samples without cladding and this contribution apparently cannot be compensated by the increased surface area of the fragmented fuel.

The results obtained can be used to estimate the relative contributions from gap or fissures and grain boundaries. A model was developed to deconvolute the various fractions [49]. The diffusion of water in the fissures and grain boundaries is assumed to be a potential rate controlling mechanism [48]. The effective modeling of the leach test results is out of the scope of this paper.

The mobilization rates of cesium and iodine decrease with time in the leach tests, as shown in Figs. 19–22. Due to the limited time availability for laboratory experiments, extrapolation supported by modeling is necessary to estimate the time required for the complete release of IRF nuclides. In absence of a suitable mechanistic model, equation (2) - with the parameters fitted by the linear regression as shown in Figs. 21 and 22 - can be used for this purpose. Integration of equation (2) for the cesium and iodine release, with b = −1.12 (for Cs) and b = −0.99 (for I), shows that the cumulated release after 1 year would represent about 90% of the expected cumulated release after 2 years. For the tests with open segments, fragments or powder, the rate is expected to decrease faster. Extrapolation of the equation to the longer term may overestimate the release, because of the probable depletion of the radionuclide source.

5. Conclusions

The FIRST-Nuclides project has extended the experimental database on the fast release by leach tests with BWR and PWR spent nuclear fuels. The gathered data allow now extension to high burn-up fuels. The fast release of iodine and cesium is comprised mainly in the range below the FGR (for I) or below 0.6 × FGR (for Cs), in agreement with theoretical considerations. Exceptions to this rule were found, which can be explained by differences in sample preparations and test durations (short term tests may not give the entire IRF), incomplete reactor operation data, and partly by artifacts in analytical procedures.

Although most experiments were done under oxidizing conditions, the contribution of oxidative fuel matrix dissolution as measured by the U concentrations in the leachates was relatively small, except for the tests with fuel powders. The existence of a continuous fission gas release mechanism and parallel iodine release mechanism during the leaching was demonstrated, but it is not yet clear to which extent this process is influenced by the fuel production process, fuel properties, sample preparations or leach conditions. The cesium and iodine release in the leaching experiments could be qualitatively correlated to the exposed surface areas. Closure of the fuel-cladding gap slows down the release. For a clear distinction between gap and grain boundary contributions, data treatment with specific mechanistic models is required. The release rate evolution was fitted with an empirical equation ($Rate = A \times t^{-b}$). Extrapolation shows that most of the segregated cesium and iodine inventories found in the free volume (gap, fractures and grain boundaries) can be mobilized in the first years after contact of the fuel samples with water.

One major finding of the FIRST-Nuclides project was the establishment of a positive correlation between cesium and iodine fast release data and linear power ratings exceeding 200 W cm^{-1}. This correlation may be used as an estimator of IRF values in safety assessment calculations for radioactive waste repository sites. The reliability of the estimation may be improved in the future if local power rating data referring to the samples become available. The data presented in this paper provide a basis to reconsider the reference IRF values in performance assessment.

Acknowledgement

The research leading to these results has received funding from the European Atomic Energy Seventh Framework Programme FP7/2007/2011 under grant agreement n°295722 (FIRST-Nuclides project).

Appendix A. Supplementary data

Supplementary data related to this article can be found at http://dx.doi.org/10.1016/j.jnucmat.2016.10.048.

Appendix A

A.1 Comment on the testing of an alternative rate equation

The decrease of the IRF release rate is described by equation (2) in the paper, i.e. $Rate = A \times t^{-b}$. An important draw-back of this equation is that the rate becomes infinite for very small times t. An alternative equation was therefore tested as well, namely $Rate = A \times e^{-bt}$. This is the type of equation used also by Casas et al. [57]. For time = 0, this expression returns Rate = A, so that A gets the physical meaning of 'rate at time zero'. The alternative equation can be written also as $log\,(Rate) = log\,A - bt$. So a plot of log (Rate) as a function of time should give a straight line. This is clearly not the case, as illustrated in Fig. 1 of this appendix, showing the data of Fig. 22 of the paper, but with a linear time scale. So apparently, using only one exponential term, this equation is not the most appropriate one. A more elaborated equation with several exponential terms, corresponding to different fractions of leachable iodine, as applied in Ref. [57] may give a better fit, but the effective modeling of the leach test results is out of the scope of this paper.

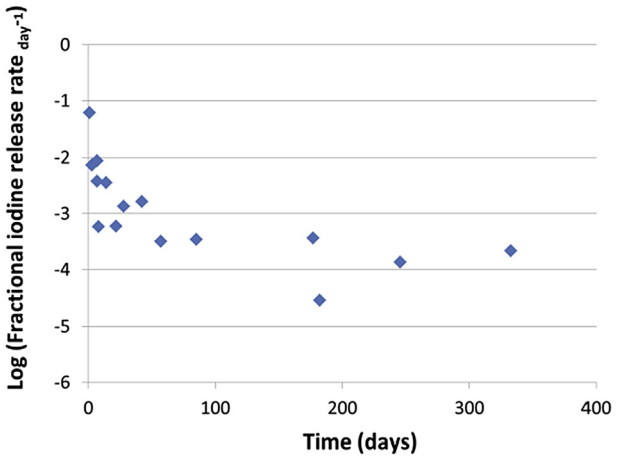

Fig. 1. Appendix: Logarithm of the fractional iodine release rate (day^{-1}) as a function of time (linear time scale) for the leach tests with clad PWR fuel Segments (S) of FIRST-Nuclides, showing a non-linear behavior, incompatible with the alternative rate equation of the type $log\,(Rate) = log\,A - bt$; the data are shown also in Fig. 22 in the paper as a function of log (time).

A.2 Comment on the theoretical diffusion behavior of Cs versus fission gasses

According to the models developed by Booth [58] and Speight [59], the diffusion of fission gases from the grain bulk to the grain boundaries, assuming that the grains are spherical and that no changes take place that would alter the diffusion geometry, is described by equation of the type

$$F = k \times \sqrt{\left(\frac{D}{a^2} \times t\right)} - k' \times \frac{D}{a^2} \times t \quad (3)$$

with F = the fraction of fission gases diffused to the grain boundary, D is the diffusion coefficient, a is the grain radius, k and k' are constants, and t is time. The equation can be simplified for lower values of F by neglecting the second term, implying that the fraction diffused out is proportional to the square root of time in this region. At higher values for F, the simplification increasingly overestimates F. Assuming that the diffusion kinetics for Cs can be described by the same equation, considering that $D_{Cs}/D_{Xe} = 0.33$ [45], and assuming that grain boundary release dominates IRF(Cs), the ratio IRF (Cs)/FGR, should thus be equal to $\sqrt{0.33}$ for lower FGR. In the given hypotheses, and if the investigated fuel sample did not have a local FGR that is much different from the FGR given by the operator, we can thus expect a slope of $\sqrt{0.33}$ (~0.6) for the fractional Cs release as a function of the FGR in leach tests. It is, however, not clear if the mentioned conditions under which the models of Booth and Speight are valid are applicable to the fuel samples tested in FIRST-Nuclides. For this reason, it was preferred to refer in the paper only to the Cs-Xe graph from Lassmann et al. [45], showing indeed a Cs/Xe ratio of approximately 0.6 up to about 60% Xe release, and not to the value $\sqrt{0.33}$ based on the theoretical models of Booth and Speight, although the values are more or less identical (which is due also to the fact that the 0.33 comes from the paper of Lassmann).

A.3 Comment on the multicorrelation of the IRF with burn-up and linear power rating

As mentioned in the paper, current correlations for IRF release are typically based on burn-up, whereas correlating to LPR seems more appropriate in view of the current data. This is ascribed to LPR being directly correlated to fuel temperature. It is true that diffusion of fission products is driven by temperature, but also time is involved and cannot be neglected. An improved correlation should account for both. If we assume that the limiting process is diffusion to grain boundaries, the fission product release is proportional to $\sqrt{(Dt)}$ according to equation (3) (under the mentioned assumptions, and if the second term can be neglected under a reasonable approximation). Under the same assumption of constant conditions throughout irradiation, this is also proportional to $\sqrt{(D \times BU)}$, with BU being the burn-up. The diffusion coefficient follows an Arrhenius dependency upon temperature (see, *e.g.* [60]).

Hence, equation (3) could be extended to

$$F = K \times e^{\left(-\frac{A}{T}\right)} \times \sqrt{(B \times BU)} \quad (4)$$

where T is the temperature and K, A and B are constants. T can be replaced by the average LPR under reasonable assumptions, since the fuel central temperature is approximately proportional to the LPR. Hence, a correlation of the type

$$F = K \times e^{\left(-\frac{A}{LPR}\right)} \times \sqrt{(B \times BU)} \quad (5)$$

could be developed, with the constants fitted on experimental data. This would account for the effect on the IRF of both burn-up and LPR.

Application of such model to the IRF data for iodine and cesium from FIRST-Nuclides was only partially successful. The model implies an increase of the IRF with LPR and with burn-up. The increase with the LPR was confirmed, as shown already by Fig. 32 in the paper. The increase with burn-up was not confirmed, though. The combined effect of LPR and burn-up is illustrated in Fig. 2 of this appendix. The data for MOX were not included. Mind that the burn-up and LPR axes are not proportional, but just show the increasing values as categories. The spatial difference between consecutive LPR or burn-up values on the graph does not reflect the actual difference in LPR or burn-up. In a proportional presentation, the LPR and burn-up axes of the graph would be more stretched. Fig. 2 nevertheless shows clearly that IRF(I) tends to increase with increasing LPR (in agreement with Fig. 32 in the paper), but that there is no clear increase with burn-up. In the higher LPR region, the data even suggest a decrease of IRF(I) with increasing burn-up. The results for IRF(Cs) indicate a similar trend (data not shown). The fact that the expected trend as a function of burn-up is not visible, may be due to the lack of IRF data for fuels with both high burn-up and high LPR, where we expect the highest combined effect. The current data set is thus not sufficient to calibrate a model based on equation (5).

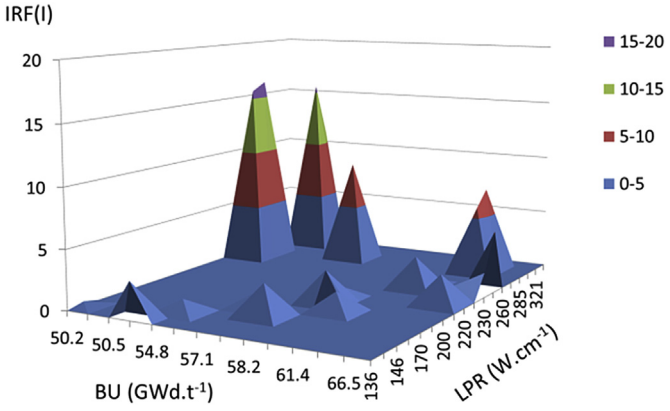

Fig. 2. appendix. IRF(I) for the FIRST-Nuclides data set, plotted as a function of burn-up (BU) and linear power rating (LPR).

References

[1] D.R. Olander, Fundamental Aspects of Nuclear Reactor Fuel Elements, National Technical Information Service, U. S. Department of Commerce, Springfield, Energy Research and Development Administration, 1976. Virginia 22161: Technical Information Center, Office of Public Affairs.
[2] K.-H. Neeb, The Radiochemistry of Nuclear Power Plants with Light Water Reactors, de Gruyter, Berlin, 1997.
[3] P. Van Uffelen, R.J.M. Konings, C. Vitanza, J. Tulenko, in: D.G. Cacuci (Ed.), Handbook of Nuclear Engineering, Springer Science+Business Media LLC, 2010, pp. 1519–1627.
[4] M. Oguma, Nucl. Eng. Des 76 (1) (1983) 35–45.
[5] J. Spino, K. Vennix, M. Coquerelle, J. Nucl. Mater 231 (3) (1996) 179–190.
[6] H. Matzke, J. Spino, J. Nucl. Mater 248 (1997) 170–179.
[7] V.V. Rondinella, T. Wiss, Mater. Today 13 (12) (2010) 24–32.
[8] H. Kleykamp, J.O. Paschoal, R. Pejsa, F. Thommler, J. Nucl. Mater 130 (1985) 426–433.
[9] L. Johnson, N.C. Garisto, S. Stroess-Gascoyne, Proc. Waste Manag. (1985) 479–482.
[10] K. Spahiu, L. Werme, U.B. Eklund, Radiochim. Acta 88 (9–11) (2000) 507–511.
[11] P. Carbol, P. Fors, T. Gouder, K. Spahiu, Geoch. Cosmochim. Acta 73 (2009) 4366–4375.
[12] Nagra, Project Opalinus Clay – Safety Report, in: Demonstration of Disposal Feasibility for Spent Fuel Vitrified High-level Waste and Long-lived Intermediate-level Waste (Entsorgungsnachweis), 2002. Nagra NTB 02–05, Nagra, Wettingen, Switzerland.
[13] SKB, Long-term Safety for the Final Repository for Spent Nuclear Fuel at Forsmark. Main Report of the SR-site Project, Updated 2012-12, in Technical Report, Svensk Kärnbränslehantering AB, SKB, Stockholm, Sweden, 2011.
[14] L.H. Johnson, L. Werme, M.J. Apted, Technology and safety factors in evaluating spent fuel as final waste form, Draft report, IAEA Consulants Meeting, 1987.
[15] S. Stroes-Gascoyne, L.H. Johnson, D.M. Sellinger, Nucl. Tech. 77 (3) (1987) 320–330.
[16] C. Ferry, P. Lovera, C. Poinssot, L. Johnson, Mater. Res. Soc. Symp. Proc. 807 (2003) 35–40.

[17] L. Johnson, C. Poinssot, C. Ferry, P. Lovera, Estimates of the Instant Release Fraction for UO_2 and MOX Fuel at t=0, 2004. Technical Report, NTB 04–08 Nagra, Wettingen, Switzerland.
[18] L. Johnson, C. Ferry, C. Poinssot, P. Lovera, J. Nucl. Mater 346 (2005) 56–65.
[19] C. Poinssot, C. Ferry, M. Kelm, B. Grambow, A. Martínez Esparza, L. Johnson, Z. Andriambololona, J. Bruno, C. Cachoir, J.M. Cavedon, H. Christensen, C. Corbel, C. Jegou, K. Lemmens, A. Loida, P. Lovera, F. Miserque, J. de Pablo, A. Poulesquen, J. Quiñones, V.V. Rondinella, K. Spahiu, D. Wegen, Final Report of the European Project Spent Fuel Stability under Repository Conditions, CEA-R-6093, Saclay, 2005.
[20] C. Poinssot, C. Ferry, B. Grambow, M. Kelm, K. Spahiu, A. Martínez, L. Johnson, E. Cera, J. de Pablo, J. Quinones, D. Wegen, K. Lemmens, T. McMenamin, Mater. Res. Soc. Symp. Proc. 932 (2006) 421–432.
[21] L. Johnson, I. Günther-Leopold, J.K. Waldis, H.P. Linder, J. Low, D. Cui, E. Ekeroth, K. Spahiu, L.Z. Evins, J. Nucl. Mater 420 (2012) 54–62.
[22] I. Matsson, B. Grapengiesser, B. Andersson, Appl. Rad. Isot. 65 (2007) 36–45.
[23] S. Holcombe, S.J. Svärd, K. Eitrheim, L. Hallstadius, C. Willman, Nucl. Tech. 184 (1) (2013) 96–106.
[24] P. Blair, A. Romano, Ch. Hellwig, R. Chawla, J. Nucl. Mater 350 (3) (2006) 232–239.
[25] P. Blair, Modelling of fission gas behavior in high burnup nuclear fuel, in Laboratoire de physique des réacteurs et de comportement des systèmes, École Polytechnique Fédérale, Lausanne, Switzerland, 2008, p. 188.
[26] B. Kienzler, E. González-Robles, V. Metz, A. Valls, L. Duro, 14th International High-level Radioactive Waste Management Conference (IHLRWMC 2013): Integrating Storage, Transportation, and Disposal, vol. 1, 277–283.
[27] E. Ekeroth, D. Cui, J. Low, M. Granfors, H.U. Zwicky, K. Spahiu, L. Zetterström Evins, Mater. Res. Soc. Symp. Proc. 1475 (2012) 125–130.
[28] A. Puranen, M. Granfors, O. Roth, KIT Scientific Report KIT-SR 7716, 2016, pp. 81–90.
[29] E. Curti, A. Froideval-Zumbiehl, M. Martin, A. Bullemer, I. Günther-Leopold, A. Puranen, D. Jädernäs, O. Roth, D. Grolimund, C.N. Borca, A. Velea, KIT Scientific Report KIT-SR 7716, 2016, pp. 135–146. Karlsruhe, Germany.
[30] E. Curti, A. Puranen, D. Grolimund, D. Jädernas, D. Sheptyakov, A. Mesbah, Environ. Sci. Process. Impacts 17 (2015) 1760–1768.
[31] D. Serrano-Purroy, L. Aldave de las Heras, S. Van Winckel, A. Martínez Torrents, R. Sureda, J.P. Glatz, V. Rondinella, KIT Scientific Report KIT-SR 7716, 2016, pp. 109–121. Karlsruhe, Germany.
[32] A. Martínez-Torrents, R. Sureda, J. de Pablo, F. Clarens, D. Serrano-Purroy, L. Aldave de las Heras, I. Casas, KIT Scientific Report KIT-SR 7716, 2016, pp. 157–168. Karlsruhe, Germany.
[33] E. González-Robles, M. Lagos, E. Bohnert, N. Müller, M. Herm, V. Metz, B. Kienzler, KIT Scientific Report KIT-SR 7716, 2016, pp. 91–97. Karlsruhe, Germany.
[34] E. González-Robles, M. Fuß, E. Bohnert, N. Müller, M. Herm, V. Metz, B. Kienzler, Mater. Res. Soc. Symp. Proc. 1744 (2015) 35–41.
[35] E. González-Robles, V. Metz, D.H. Wegen, M. Herm, D. Papaioannou, E. Bohnert, R. Gretter, N. Müller, R. Nasyrow, W. de Weerd, T. Wiss, B. Kienzler, J. Nucl. Mater 479 (2016) 67–75.
[36] E. Curti, I. Günther-Leopold, H.-P. Linder, N. Milosavljevic, KIT Scientific Report KIT-SR 7716, 2016, pp. 123–133. Karlsruhe, Germany.
[37] O. Roth, Ch. Askeljung, A. Puranen, M. Granfors, D. Cui, J. Low, KIT Scientific Report KIT-SR 7716, 2016, pp. 189–199. Karlsruhe, Germany.
[38] O. Roth, A. Puranen, Ch. Askeljung, D. Cui, KIT Scientific Report KIT-SR 7716, 2016, pp. 29–39. Karlsruhe, Germany.
[39] T. Mennecart, K. Lemmens, C. Cachoir, KIT Scientific Report KIT- SR 7716, 2016, pp. 147–156. Karlsruhe, Germany.
[40] E. Slonszki, Z. Hózer, KIT Scientific Report KIT- SR 7716, 2016, pp. 169–179. Karlsruhe, Germany.
[41] H. Bailly, D. Ménessier, C. Prunier, The Nuclear Fuel of Pressurized Water Reactors and Fast Reactors Design and Behaviour, Lavoisier Publishing, Paris, France, 1999. CEA 2-7272-0198-2.
[42] Y. Bentor, Chemical Elements (Formerly "The Periodic Table of the Elements on the Internet"), 2012. http://www.chemicalelements.com/index.html.
[43] D.R. Olander, P. Van Uffelen, J. Nucl. Mater 288 (2–3) (2001) 137–147.
[44] B.J. Lewis, C.E.L. Hunt, F.C. Iglesias, J. Nucl. Mater 172 (1990) 197–205.
[45] K.A. Lassmann, A. Schubert, J. van der Laar, C.T. Walker, On the diffusion coefficient of cesium in UO_2 fuel, fission gas behavior of water reactor fuels, in: Seminar Proc. 26–29 September 2000, NEA, 2002, pp. 321–334.
[46] S.G. Popov, J.J. Carbajo, V.K. Ivanov, G.L. Loder, Thermophysical Properties of MOX and UO2 Fuels Including the Effect of Irradiation, Oak Ridge National Laboratory (ORNL), 2000. Report TM-2000/351.
[47] B.V. Dobrov, O.V. Khoruzhii, S.Yu Kourtchatov, V.V. Likhanskii, Nucl. Eng.Des 195 (3) (2000) 361–371.
[48] M. Pekala, Andres Idiart, Lara Duro, KIT Scientific Report KIT- SR 7716, Karlsruhe, Germany, 2016, pp. 211–221.
[49] I. Casas, A. Espriu, D. Serrano-Purroy, A. Martinez-Esparza, J. De Pablo, KIT Scientific Report KIT-SR 7716, 2016, pp. 227–236.
[50] M. Verwerft, B. Vos, S. Van den Berghe, K. Govers, SCK•CEN Report R-5579, 2014.
[51] O. Roth, J. Low, K. Spahiu, Mater. Res. Soc. Symp. Proc. 1665 (2014) 261–266.
[52] H. Curtius, N. Lieck, G. Kaiser, M. Güngör, M. Klinkenberg, D. Bosbach, KIT Scientific Report KIT-SR 7716, Karlsruhe, Germany, 2016, pp. 59–67.
[53] H. Curtius, G. Kaiser, N. Lieck, M. Güngör, M. Klinkenberg, D. Bosbach, Radiochim. Acta 103 (6) (2015) 433–442.
[54] D. Serrano-Purroy, I. Casas, E. González-Robles, J.P. Glatz, D.H. Wegen, F. Clarens, J. Giménez, J. de Pablo, A. Martínez-Esparza, J. Nucl. Mater 434 (1–3) (2013) 451–460.
[55] D. Serrano-Purroy, F. Clarens, E. González-Robles, J.P. Glatz, D. Wegen, J. de Pablo, I. Casas, J. Giménez, A. Martínez, J. Nucl. Mater 427 (2012) 249–258.
[56] H. Assmann, Advantages of Oxidative UO_2 Sintering Process "NIKUSI". European Nuclear Society Meeting (ENC'86), June 1-6, 1986, Geneva, CH, 1986.
[57] I. Casas, A. Espriu, D. Serrano-Purroy, A. Martinez-Esparza, J. De Pablo, KIT Scientific report KIT-SR 7676, Karlsruhe, Germany, 2014, pp. p.139–145.
[58] A.H. Booth, A method of calculating fission gas diffusion from UO2 fuel and its application to the X-2-f test, report CRDC-721, AECL N°496, 1957.
[59] M.V. Speight, A calculation on the migration of fission gas in material exhibiting precipitation and Re-solution of gas atoms under irradiation, Nucl. Sci. Eng. 37 (1969) 180–185.
[60] Lassmann, Benk, J. Nucl. Mater 280 (2000) p.127–135.